The Thesis Committee for Peter Mark Tutton
Certifies that this is the approved version of the following Thesis:

Carbon Capture and Storage Network Optimization Under Uncertainty

APPROVED BY
SUPERVISING COMMITTEE:

Benjamin D. Leibowicz, Supervisor

Susan D. Hovorka, Co-Supervisor

Carey W. King, Reader

Carbon Capture and Storage Network Optimization Under Uncertainty

by

Peter Mark Tutton

Thesis

Presented to the Faculty of the Graduate School of

The University of Texas at Austin

in Partial Fulfillment

of the Requirements

for the Degree of

Master of Science in Energy and Earth Resources

The University of Texas at Austin

May 2018

Acknowledgements

Firstly, I would like to thank Fulbright for their sponsorship of my studies. I would also like to thank my supervisors, Dr. Benjamin Leibowicz and Dr. Susan Hovorka, and reader, Dr. Carey King, for the guidance and expertise they have offered me throughout my thesis. Additionally, all of the staff and students at the Gulf Coast Carbon Center have provided valuable insights that have helped to shape my work. Finally, I would like to express my gratitude to Mr. Richard Chuchla and Ms. Jessica Smith for all the help, advice and patience they have shown over the past two years.

Funding to support this research was provided in part from the Department of Energy co-operative agreement DE-FE0029487, titled CarbonSAFE Phase I: Integrated CCS Pre-Feasibility – Northwest Gulf of Mexico, with Dr. T. A. Meckel as the principal investigator.

Abstract

Carbon Capture and Storage Network Optimization Under Uncertainty

Peter Mark Tutton, M.S.E.E.R.

The University of Texas at Austin, 2018

Supervisors: Benjamin D. Leibowicz, Susan D. Hovorka

Carbon capture and storage is a method for emissions reductions that can be applied to both the electric sector and industrial sources. Significant uncertainties surround the technologies, policy and extent to which CCS will be deployed in the future. For widespread deployment, future CCS demand should be considered during infrastructure planning.

This study presents a novel model that considers spatial information and uncertainty in generating an optimal CCS network. The two-stage stochastic model, utilizes both geographic information systems (GIS) and mixed integer programming (MIP), to generate an optimal near-term hedging strategy. The strategy considers one discrete uncertainty distribution: the future demand for CO_2 storage.

A case study in the Texas Gulf Coast demonstrates the value of considering uncertainty of future demand. The optimal solution is selected from a candidate network consisting of twelve sources and five reservoirs that can be linked via a network of pipelines and ship routes. The results demonstrate that optimal hedging strategies lead to transportation cost savings of up to 14% compared to a 'naïve approach' in which only the

expected value is considered. The transportation selection also highlights the benefit of utilizing ship transport in uncertain scenarios due to their ability to be reassigned to a different route or sold.

Table of Contents

List of Tables

List of Figures

Chapter 1: Introduction

Greenhouse gas emissions from anthropogenic sources are at an historical high (IPCC, 2014). Elevated levels of these gases, such as carbon dioxide (CO_2), have had widespread impacts on global temperatures, ice sheets and sea-levels. In order to mitigate risks from climate change, the atmospheric concentration of these greenhouse gases has to be reduced. Emissions reductions can be brought about in three ways: energy use reduction, carbon intensity reduction or increase carbon capture and storage (Bachu, 2003).

Carbon capture and storage (CCS) is the process of removing CO_2 from emissions sources and transporting it to a storage location where it remains separate from the atmosphere over significant periods of time. CCS consists of three major subsystems: capture, transportation and storage. The Intergovernmental Panel on Climate Change describes the need for CCS, as part of the many possible global mitigation strategies, if warming is to be limited to below 2ºC compared to pre-industrial levels (IPCC, 2014). Without CCS, the IPCC estimates the costs of reaching this goal could be 138% higher. Kriegler et al. (2014) note that CCS provides the most valuable technology across multiple mitigation scenarios due to its ability to be applied to emissions from both the electric and non-electric sectors. In spite of this, there exists no consensus over how CCS will be implemented and to what extent.

Future climate change policy is likely to have a large impact on the development of CCS projects. The United States recently amended the Section 45Q tax credits for CCS (26 USC 45Q), which provide up to USD$50, or USD$35, for each tonne of CO_2 stored geologically or retained during enhanced oil recovery (EOR) utilization respectively. These credits can be claimed for 12 years from the beginning of service, for capture facilities that start construction before 2024. However, the benefits past this point are unknown. This

represents just one of the many uncertainties surrounding future drivers for emissions reductions. The future stringency of CO_2 emissions caps, or prices on carbon, will directly influence the demand for CCS projects (IEA, 2013).

To date, only a few CCS projects have resulted from policy drivers, with Sleipner and Snøhvit providing early examples of development incentivized by a price on carbon (IEA, 2011a). Instead, the majority of projects to date have been implemented via utilization within EOR. The revenues from this pathway provide the necessary economics for the majority of current large-scale CCS development, see Figure 1.

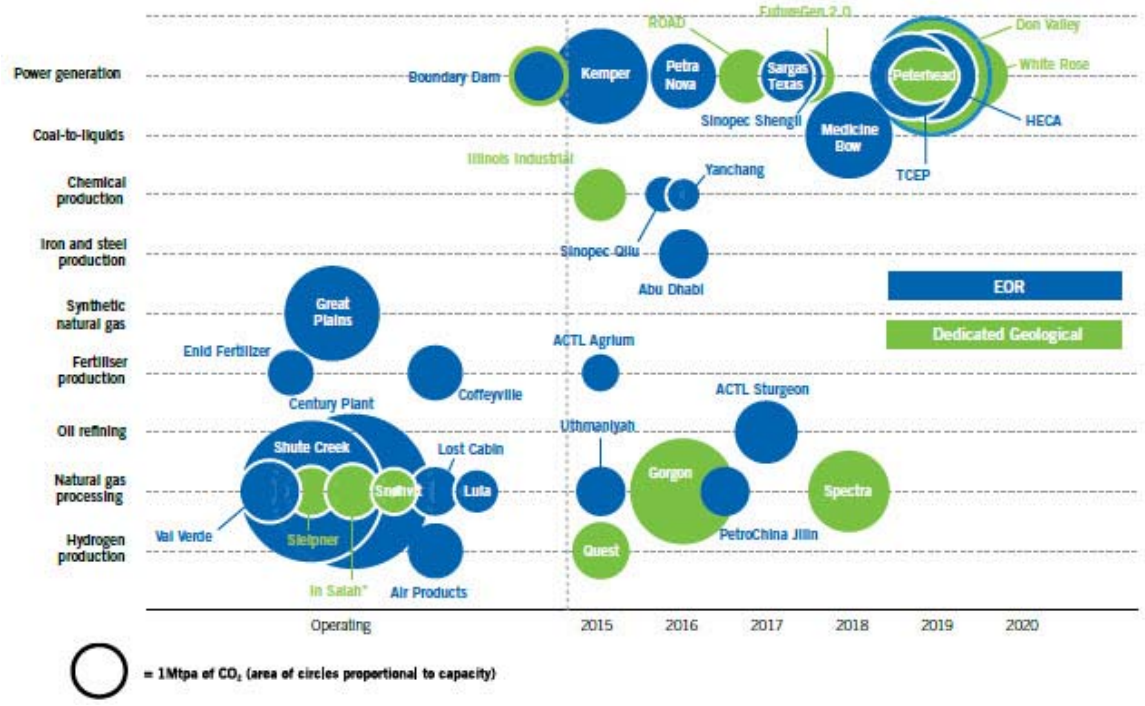

Figure 1. Large scale integrated CCS projects, displaying industry and storage formation type (GCCSI, 2014)

These projects provide an insight into implementation of technologies within the full CCS chain. However, they have predominantly focused on capturing CO_2 from one

source and transferring it to a single reservoir (IEA, 2011). For large scale CCS implementation, it is likely that networks which aggregate CO_2 from multiple sources and link them to multiple storage reservoirs will be used. Integrated networks provide the opportunity to capture economies of scale (IEA, 2011; Kuby et al, 2011) as well as provide resiliency against supply disruptions (Essandoh-Yeddu and Gülen, 2009; Fimbres Weihs et al., 2011; IEAGHG, 2010), but with the tradeoff of higher up-front costs. This type of network has been demonstrated in the oil and gas sector. However, due to the lack of experience with this type of network in CCS, there are significant uncertainties regarding the implementation for CCS.

Significant value can be captured by optimizing the infrastructure network. Within different climate change mitigation strategies, it is expected that the total investment in CCS, until 2050, could range from USD 1.4 trillion to 2.8 trillion (GCCSI, 2013). These high costs, along with high risks, currently present an obstacle to CCS deployment (ZEP, 2011b). A 'wait and see' approach is often taken by decision makers to try and reduce risk associated with the possible options (Lee et al., 2017). However, a common theme throughout the literature describes the need to pass on cost reductions by planning infrastructure that considers both short-term and long-term CCS targets (GCCSI, 2013; IEA, 2013; Ozaki et al., 2013). Additionally, the planning should consider the ability to integrate existing infrastructure into these networks (Middleton et al., 2012). Leveraging existing infrastructure not only reduces costs, but also speeds up development and deployment of future projects (Morbee et al., 2011).

To date, some CCS network optimization models have captured spatial details or uncertainty, but never both together. Deterministic approaches fail to recognize the uncertainties related to the technological, cost and regulatory aspects of CCS projects. Whereas previous stochastic approaches neglect the importance of the spatial distribution

of sources and storage reservoirs in generating transportation options. Models have not yet considered a fully integrated network optimization that combines both the spatial and uncertainty aspects that constrain CCS deployment.

This paper presents a model to guide decision makers by showing the value in considering uncertainty in early stage decisions and infrastructure investment. The study begins by assessing the current state of technologies in each of the CCS subsystems before developing an integrated model for CCS infrastructure development considering uncertainties in future demand. It addresses one of the seven key actions described by the IEA (2013): to develop infrastructure that considers anticipated future needs. The method uses both geographic information systems (GIS) and mixed integer programming (MIP) to combine the temporal and spatial aspects of network optimization under uncertainty. A case study on the Texas Gulf Coast demonstrates a potential application of the model and the resulting value over a 'naïve' approach. The output provides information on when and where to build infrastructure as well as a visualization that can be used to aid policymakers in interpreting the results. The case study highlights several key findings including the importance of the time value of money in network build out and the role of ship transportation in scenarios with uncertain future demand for CCS.

Chapter 2: Overview

Within the three CCS sub-systems, there exist multiple different technologies and pathways for delivering integrated projects. These present tradeoffs between maturity of technology, cost and applicability to different scenarios. As such, there is no clear choice of what technologies to choose, and whether these will still be relevant for future CCS projects. The development of these technologies over the coming years, and the associated changes in price, will undoubtedly lead to variations in the future deployment of CCS.

2.1 CAPTURE

The first stage in CCS is capturing the CO_2 to increase its concentration. Higher purity CO_2 is preferred to increase the efficacy of transportation and storage. Concentrations of over 95% CO_2 are also required to ensure oil miscibility in EOR (Serpa et al., 2011). Capture usually requires the greatest investment in a project, contributing approximately 75% of the full-chain CCS costs (ZEP, 2011a; IEA, 2011a; GCCSI, 2013). Multiple different technologies and processes exist depending on the characteristics of the emissions' source.

2.1.1 Processes

The CO_2 can be captured at various points within the process stream via post-combustion capture, oxy-fuel combustion capture, and pre-combustion capture.

Post-combustion capture separates the CO_2 from flue gases after the combustion of the fuel has taken place in air (IPCC, 2005; IEA, 2013). This application predominantly lends itself to electrical power generation, but also has applications in iron and steel production. Due to the low concentrations of CO_2 in flue gases, 7-14% for coal and ~4%

for gas, there are large energy requirements to increase its concentration (Leung et al., 2014).

Oxy-fuel combustion burns the fuel in high purity oxygen instead of air. This results in a flue gas with a CO_2 concentration of 70-80%. Significant energy requirements, compared to a base case scenario, result from the necessity of an air separation unit (ZEP, 2011b). However, it produces a high-pressure CO_2 stream, therefore reducing subsequent compression costs (Blomen et al., 2009). It is the least developed of the current technologies and is associated with the greatest uncertainties (ZEP, 2011a).

Pre-combustion capture generates hydrogen, carbon monoxide and carbon dioxide from a hydrocarbon or biomass fuel. The process is known as gasification, for the case of solid fuels, or reforming, for natural gas. The CO_2 is removed from the output stream, known as synthesis gas, to leave hydrogen which can be used in combustion for power generation (IEA, 2013). Integrated gasification combined cycle (IGCC) power generation lends itself to pre-combustion capture (Leung et al., 2014). Figure 2 provides an illustration of the three different methods of capture.

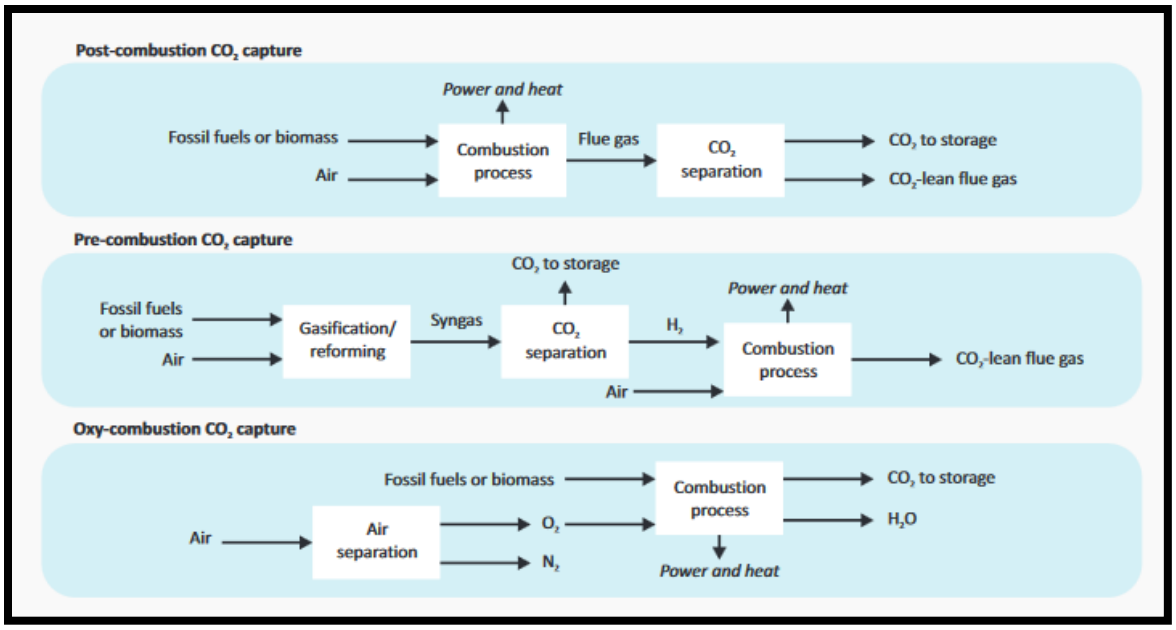

Figure 2. Schematic representation of the three processes for CO_2 capture (IEA 2012)

2.1.2 Technologies

Various technologies lend themselves to the removal of the CO_2 from the different points in the process. These fall into four main categories: absorption, adsorption, membrane separation, and cryogenic separation.

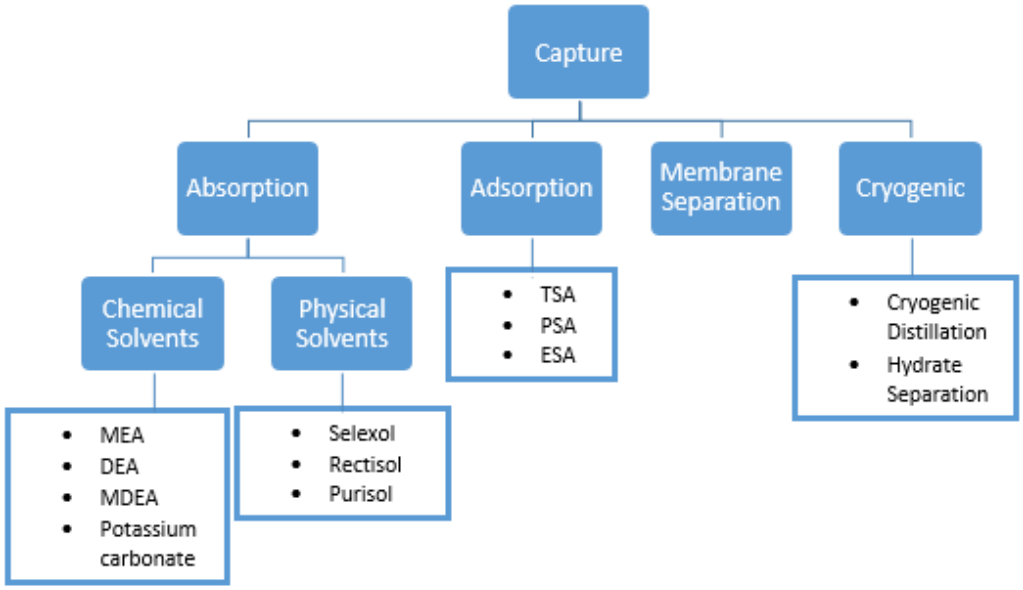

Figure 3. Tree diagram demonstrating the different types of capture technologies currently available

Absorption is currently used in many commercial applications, with monoethanolamine (MEA) used widely in industry (Ho et al., 2011). Chemical solvents are designed for CO_2 removal from gases with low pressures and low CO_2 concentrations. This makes them suited to capture from flue gas. These alkaline solvents react with the CO_2, which is an acid gas. The CO_2 can subsequently be released by heating the absorbent, and in doing so regenerating the solvent (IEAGHG, 2008). The rate of reaction, energy requirement for regeneration, and degradation in the presence of certain flue gas components vary between the different solvents (Ho et al., 2011). Therefore, the optimal choice depends on many factors including the process, electricity price, and solvent price. The regeneration heating requires a high energy consumption, 4 MJ/tonne CO_2 for MEA, and so less energy intensive solvents are likely needed in order to see large-scale CCS use

in future (Ho et al., 2011; Leeson et al., 2017). The energy cost and solvent replacement contribute 35-50% and ~10% of the total capture costs respectively (Ho et al., 2011), with solvent replacement and disposal tripling the variable operating costs for a power plant (ZEP, 2011a).

Physical solvents also absorb the CO_2, but they are suited to processes with pressures over 2 MPa and high CO_2 concentrations. Regeneration and CO_2 release is initiated by a reduction in pressure. These solvents are less affected by oxygen and nitrous oxides than chemical solvents. However, due to the optimal pressure and concentration requirements, they are not suited to post-combustion capture from flue gases. Instead these solvents are preferred in pre-combustion capture (IEAGHG, 2008).

Adsorption can also be used to selectively remove gases such as CO_2 by fixing it to the surface of a sorbent such as alumina or activated carbon (IEAGHG, 2008). Either temperature, pressure or electric currents can be used to cause the adsorption and desorption of the CO_2. Pressure swing adsorption (PSA) is commonly used in hydrogen production (IEAGHG, 2017). Hydrogen has a weak adsorbent force, so isn't adsorbed under pressure unlike CO, CO_2 and CH_4. Depressurization, desorption and regeneration of the adsorbent releases these gases. The resulting PSA tail gas usually contains 45-50% concentration CO_2 for a steam methane reformed (SMR) (IEAGHG, 2017).

The remaining two methods, membrane and cryogenic separation, are less widely used. In the former, certain gases pass across a membrane depending on the pressure difference and chemical itself. This lends itself to high concentration and high-pressure CO_2 streams. However, it has not been demonstrated on a large scale, but has potential applications in oxy-combustion (IEAGHG, 2008). Cryogenic processes are also suited to oxy-combustion and pre-combustion capture. Cooling of the gas stream is used to bring about phase changes. Provided the constituents of the gas composition have disparate

boiling points, the gases can be separated effectively using distillation (IEAGHG, 2008). In the presence of water, and under pressure, hydrate formation can be initiated (Leung et al., 2014). This provides a lower energy penalty for CO_2 separation than distillation but is currently still in the research phase.

2.1.3 Emissions Sources

The capture technology and process are dependent on many factors including the fuel and emissions source (Leung et al., 2014). The majority of attention to date has focused on capture from the flue gases associated with electricity generation (IPCC, 2005). This is in part due to coal contributing 42% of global electricity production and 28% of total CO_2 emissions (IEA, 2010). The optimal capture implementation varies between studies, depending on the assumptions and technologies used. The IEAGHG (2006) demonstrated that pre-combustion capture provides the most economic option for coal plants, at $23 per tonne CO_2 avoided. However, ZEP (2011a) showed post-combustion had the lowest avoidance costs for hard coal, whilst oxy-fuel was preferred when lignite was used. The costs for gas fired power generation are significantly higher, with an avoidance cost of $59-143 per tonne CO_2 for post combustion capture (Rubin et al., 2015). These higher costs are due to the lower emissions intensity for gas fired power plants (ZEP, 2011a).

Industrial sources also present an ideal platform for capturing CO_2. In the 2^{o}C scenario, 45% of CO_2 captured between 2015 and 2050 is predicted to come from industrial emissions (IEA, 2013). Unlike in electricity generation, there are often no low carbon alternatives in industry due to high efficiencies of the processes and CO_2 production that is inherent within the chemical process (IEA, 2013). CCS presents itself as one of the limited emissions reduction pathways in these scenarios. Industrial sources often cluster in

certain regions with developed land and water transportation access providing opportunities for an integrated infrastructure to be leveraged (Leeson et al., 2017).

Industrial sources can be broken down into five groups: high purity sources, biomass conversion, cement production, iron and steel production, and refineries (IEA, 2011a). Iron and steel had the largest overall contribution to industrial emissions, with 31%, followed by cement production, 27%, and refineries, 10% (IEA, 2011a). Biomass conversion presents the valuable option to generate electricity with negative CO_2 emissions, by utilizing CCS (Kriegler et al., 2014). However, the impact on food supplies and sustainability of this method needs to be considered (IEA, 2011a).

Due to the wide range of processes, the cost of capture in industry demonstrates a high variability with prices ranging from $20-120 per tonne of CO_2 avoided (Leeson et al., 2017). Boilers, furnaces and kilns are responsible for a large portion of the total emissions. These diluted CO_2 streams are similar to post-combustion capture from power plants (IEA, 2011a). However, certain processes, such as hydrogen production at refineries, produce higher purity CO_2.

High purity sources present opportunities for early stage development projects. The sources either generate high concentrations of CO_2 as a by-product or utilize CO_2 removal to increase the purity of the primary product. In certain circumstances, the cost of capture can be reduced to under $5 per tonne CO_2 (Zakkour and Cook, 2010). Many different chemical processes produce a high concentration of CO_2 including natural gas processing and liquefaction, as well as production of ammonia, ethylene oxide, ethanol, and hydrogen (Leeson et al., 2017).

2.1.3.1 Hydrogen Production

Hydrogen is used in many industrial applications including the production of ammonia. Steam methane reforming is commonly used. This process reacts natural gas and steam in the presence of a nickel catalyst to produce hydrogen and carbon monoxide.

$$CH_4 + H_2O \rightleftharpoons 3H_2 + CO$$

Additional hydrogen is produced via the water shift reaction in which water and the carbon monoxide combine to produce CO_2 and hydrogen.

$$CO + H_2O \rightleftharpoons CO_2 + H_2$$

Adsorption or absorption is commonly used to purify the hydrogen through the removal of CO_2. However, there has been a recent switch from using chemical adsorbents to purify the hydrogen stream, to using PSA. This change resulted in higher purity hydrogen and higher efficiencies, but also resulted in a less pure CO_2 stream (Lindsay et al., 2009). The CO_2 can be captured at multiple places during hydrogen production. Each is associated with a different cost of capture due to the pressure of the CO_2, concentration and temperature (Lindsay et al., 2009; IEAGHG, 2017). These costs can range from $25 to $71 per tonne CO_2 avoided, with significant variations in the total fraction of emissions captured in each case.

2.1.3.2 Gas Processing

Natural gas can contain up to 70% CO_2 when it is produced (IEA, 2011a). The CO_2 must be removed from the natural gas to meet the typical 2 – 3% by volume CO_2 pipeline

specifications defined by the operator (Berstad et al., 2012; Kinder Morgan, 2013). Three of the current saline projects, In Salah, Snøhvit and Gorgon, currently store the CO_2 removed from natural gas processing, as well as many EOR projects. For liquefied natural gas (LNG) production the limit is set at 50 ppm CO_2, to prevent freezing at the low temperatures needed to transport natural gas in a liquid state. As a result, LNG export facilities utilize CO_2 removal techniques to transform the gas from a pipeline quality to an LNG quality feed.

2.1.3.3 Ethylene Oxide Production

Ethylene oxide is an intermediate in the production of many chemicals including ethylene glycol, which go on to be used in antifreeze and as a solvent in paints and plastic production. In ethylene oxide production, ethylene reacts with oxygen over a silver catalyst surface. Two reactions occur: the partial oxidation of ethylene to produce ethylene oxide and the total oxidation of ethylene to produce CO_2 and water (Kestenbaum et al., 2002).

$$C_2H_4 + 0.5\ O_2 \rightarrow C_2H_4O$$

$$C_2H_4 + 3\ O_2 \rightarrow 2\ CO_2 + 2\ H_2O$$

Due to this reaction, the exhaust stream from ethylene oxide production contains a high concentration of CO_2 (IEA, 2011a). This process also presents itself as an economically feasible route for early-stage commercial development of CCS projects. Figure 4 demonstrates the range of different industrial capture costs.

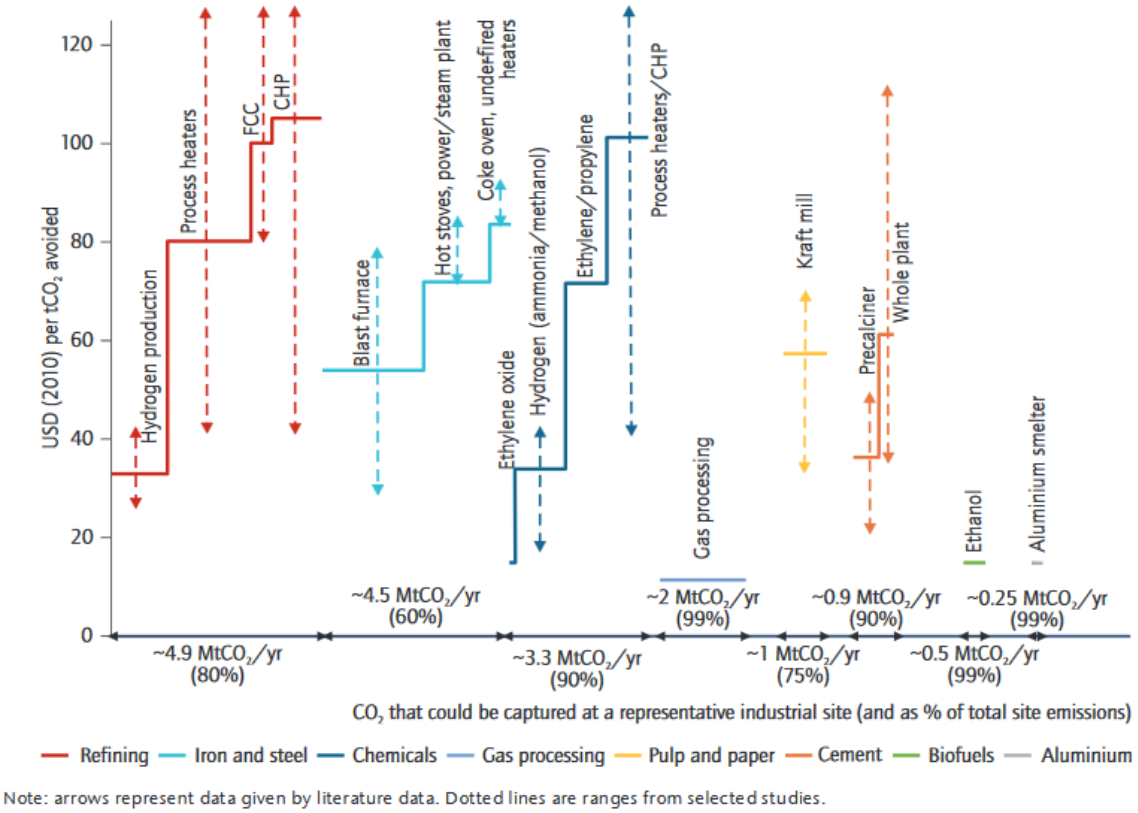

Note: arrows represent data given by literature data. Dotted lines are ranges from selected studies.

Figure 4. The cost of capturing CO_2 in several industrial processes. The horizontal length of the line demonstrates the magnitude of the emissions from different processes at an industrial source. The dashed arrows represent the range of costs from literature (IEA, 2013).

2.1.4 Conditioning

Before the CO_2 can be transported it must be conditioned and pressurized. The presence of impurities not only alters the physical properties, like critical point, of the CO_2, but can also affect the material choices. The presence of these is dependent on the fuel and the process. Hydrogen sulfide is an impurity that is common in natural gas production, which may also occur in the CO_2 stream without proper desulfurization. This presents many problems as it is toxic and can cause hydrogen embrittlement of steels (Vandeginste and Piessens. 2008).

Another common impurity is water. Water that is not dissolved in the CO_2 stream, also known as free water, can form carbonic acid, leading to the corrosion of carbon steel pipes. Conditioning of the stream to reduce the free water provides the most cost-effective solution; using stainless steels instead would increase costs by an order of magnitude (ZEP, 2011b). The acceptable amount of free water in the CO_2 stream varies widely in the literature. This limit depends on the temperature and pressures expected, and as such there is no specification. Estimates range from 20ppm (IPCC. 2005) up to 500 ppm (Buit et al., 2010), with existing projects and feasibility studies setting conservative limits: Snøhvit dehydrates to less than 50ppm and Kingsnorth proposed a limit of 24ppm (Zhou et al., 2014). However, the limits should be adjusted for offshore injection where it is feasible that temperatures could reach 4^{o}C, at which point freezing or hydrate production becomes an issue due to the potential for fouling or blockages (IEAGHG, 2004). These limits have cost implications for the dehydrating equipment and energy costs required at the point of capture.

After conditioning, the CO_2 must be pressurized to a dense phase. Figure A1 in Appendix A gives the phase diagram for pure CO_2. Transportation of dense phase CO_2 provides an efficient method to move the CO_2, with certain cases costing 30% less than transport in the gas phase (Roussanaly et al, 2013). This requires compressors and pumps to increase the pressure to above the bubble point and maintain it there throughout the transportation. The compressors pressurize the stream to the critical point and the pumps increase, and maintain, the pressure within the dense phase. This process requires large amounts of energy with compression contributing a significant percentage of total costs as the energy price increases (McCollum and Ogden, 2006). Different studies assume a range of operating conditions, with Mallon et al. stating over 8.5MPa, Heddle et al. citing 10 MPa and ZEP (2011b) up to 25 MPa offshore, with the ASME-ANSI Class #900 specification

for flanges, pipes are assumed to operate up to 15.3MPa. The entry and exit pressure of the CO_2 in the transportation network causes variations in the compression, pumping and boosting fixed and variable costs.

The cost effectiveness of capture will likely influence the demand for CCS in the future. As the prior section demonstrated, this is not only dependent on the technological development, but on other uncertain factors such as future energy costs and developing a consensus on the stringency of CO_2 conditioning.

2.2 TRANSPORTATION

The second sub-system in the CCS chain is transportation. The majority of stationary emitters of CO_2 are not collocated with a storage site. Two forms of transportation are considered for early-stage to fully-developed CCS projects: pipelines and maritime shipping.

In all cases, the most efficient transport of CO_2 occurs as a dense, single phase fluid. Transportation in this region results in a large mass flow rate for a relatively low pressure drop per unit length. Frictional losses in the pipe cause the pressure to drop. Depending on the length of the network, booster stations may be required to ensure the CO_2 stays in the dense phase. The minimum delivery pressures to the storage site are assumed throughout the literature to range between 6MPa (ZEP. 2011b) and 8.3 MPa (Farris, 1983). These pressures guarantee that the CO_2 will remain in the dense phase under the given transport conditions, irrespective of temperature and pressure fluctuations likely to be encountered.

Although CO_2 is non-flammable, it is considered a hazardous liquid due to the high pressures it is transported under. Due to its high density, in the event of a leak the CO_2 would settle in low areas and could cause asphyxiation. This presents restrictions on where pipelines can be situated, which is an important consideration in the development of a

network. However, zero fatalities have occurred from CO_2 transportation, in the USA, from 1990-2002 (IPCC, 2005).

The majority of dedicated CCS projects to date have consisted a single emissions source with a direct link to a single reservoir, see Figure 5. However, for both shipping and pipeline transport, emissions from multiple sources can be aggregated and transported via a trunk line, which then distributes the CO_2 to multiple reservoirs. This integrated network approach provides flexibility to allow maintenance breaks and unforeseen shutdowns without impacting the CO_2 supply (Essandoh-Yeddu and Gülen 2009). Shared networks also provide an economically feasible pathway, for transportation of CO_2 from small to medium scale emitters (Roussanaly et al. 2013, and IEAGHG. 2010). One such example is the Alberta Carbon Dioxide Trunk Line project which aims to capture 1.6 Mtpa CO_2 from a fertilizer plant and refinery for use in EOR. A further 13 Mtpa capacity is planned, so that additional CO_2 streams can be received by the network (IEAGHG, 2015).

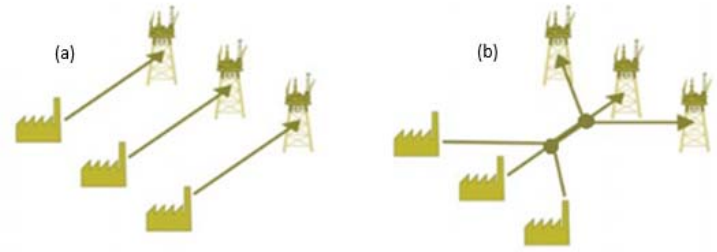

Figure 5. A schematic illustrating (a) direct link infrastructure, and (b) networked infrastructure (adapted from IEAGHG, 2010).

2.2.1 Pipelines

There is extensive experience with pipeline transport in the US, for both natural gas and also CO_2. Pipelines have been used to carry CO_2, for enhanced oil recovery (EOR), since the construction of the Canyon Reef pipeline in 1972 and currently there are 50 CO_2

pipelines totaling over 4500 miles. However, 80% of these transport CO_2 from natural sources and are used for EOR (NETL, 2015). The majority of these were built between the 1980s and 1990s, however new systems are still being built.

This network is expected to grow dramatically, if a carbon tax were implemented, with 1000 miles added on average until 2030 and anthropogenic CO_2 use growing to make up 85% of that used in EOR (NETL. 2015). Point to point networks have been studied due to their simplicity. However, they often present a sub-optimal solution with regards to long term CCS targets (ZEP. 2011b). Clustering and aggregation of sources can be applied to 60% of potential networks globally, equating to 46% savings in length of installed pipeline and 19% in the USA (IEAGHG, 2010).

Figure 6. The geographical distribution of CO_2 pipelines U.S. (Melzer, 2011).

Transportation costs can make up to 30% of the total CCS investment (Fimbres Weihs et al., 2014). The cost of building pipeline infrastructure is not only dependent on pipeline diameter and length, but also on factors such as terrain and land use (IEAGHG,

2010, McCoy and Rubin, 2008, and Heddle et al., 2003). The costs for transportation via pipeline can be broken down into the following categories (NETL, 2014 and ZEP, 2011b): materials, labor, rights of way (ROW), and miscellaneous. The miscellaneous category contains a range of cost factors including surveying engineering, contingencies, and CO_2 metering.

Due to the limited data on CO_2 pipelines, many studies have instead used natural gas pipelines as analogies for calculating CO_2 transportation costs (Heddle et al. 2003, and McCoy and Rubin, 2008). However, Mallon et al. (2013) note that the costs between the two systems can deviate significantly. Due to the corrosive nature of impure CO_2 it was suggested they could incur a 10% premium over natural gas pipelines (Essandoh-Yeddu and Gülen, 2009).

The majority of pipeline cost approximations calculate the capital cost as a function of pipeline diameter and length. However, Parker (2004) and Roussanaly et al. (2013) disaggregated the costs, based on the materials, labor, right of way and miscellaneous expenses. The resulting interactions vary, with Parker (2004) showing the pipeline cost per unit length increasing with increasing diameters, whereas McCoy and Rubin (2008) and Vandeginste and Piessens (2008) showed the same increase with diameter, but an economy of scale with total length. Economies of scale can be seen for materials, labor, and miscellaneous costs for both length and diameter. Rights of way only exhibit economies of scale with diameter (McCoy and Rubin, 2008).

Using the data in Table 1 for two recently completed CO_2 pipelines, the Green and Greencore pipelines, NETL (2014) evaluated the accuracy of cost prediction models. It was shown there are large discrepancies between predicted and the actual values, with the majority underestimating the costs. The models of Parker (2004) and McCoy and Rubin (2008) provided the closest estimates. McCollum and Ogden (2006) also compared

multiple cost estimations, showing there was up to a factor of five difference between different models.

Table 1. Summary of details for the two CO_2 pipelines, the Green and Greencore, completed since 2010

Pipeline	Length (miles)	Diameter (inches)	Price ($ million)
Green	314	24	884
Greencore	232	20	285

Multiple reasons for the discrepancies in costs include the volatility of pipeline prices as well as the regional variation in costs. Pipeline costs doubled from 2011-2013 as a result of increased miscellaneous costs and competition for labor (Smith, 2014). In concert with this, labor costs also show a significant difference between regions in the USA. Several studies showed the importance of region specific cost estimations (McCoy and Rubin, 2008 and NETL. 2015). If large scale deployment of CCS projects occurs, along with the forecasted LNG growth, the competition between the two industries for a limited resource is likely to push pipeline prices even higher (GCCSI, 2013). The trend is not always an increasing one with material costs increasing by a factor of 4 between 2004 and 2009 (Mallon et al. 2013 and ZEP. 2011b), yet reducing marginally from 2012 to 2013 (Smith, 2014). Escalation factors are sometimes included to account for temporal changes in the market prices (Essandoh-Yeddu and Gülen, 2009).

Methodologies to minimize these costs by choosing an optimal route have also been developed (Heddle et al., 2003). Different land use and terrain provide significant increases in the construction costs of pipelines, with up to a factor of 10 increase in populated areas. Avoiding such areas or following existing routes has the ability to reduce costs as well as permitting times. Although these factors only apply to onshore transport, offshore transport

has similar scope for optimization as seafloor topography and shipping lane routes can influence the chosen path (ZEP. 2011b). Bends and deviation in the route were found to have a much smaller effect than changes in topography (Vandeginste and Piessens. 2008).

Permitting is likely to impact both the cost and time to completion for onshore projects because the federal government has no power of eminent domain for CO_2 pipelines (NETL, 2015). This is in contrast to certain states, where eminent domain can be provided for CO_2 pipelines in certain circumstances (NETL, 2017). Re-use of existing natural gas pipelines could mitigate these issues though. FEED studies for implementing CCS to Longannet power station in the UK, demonstrated a scenario in which existing pipelines could be reused (Zhou et al., 2014). Reuse only provides a limited cost saving, over a new pipeline, as numerous factors, including remaining life, operating pressure and recertification, need to be considered (Serpa et al., 2011). In addition, offshore construction has a reduced permitting time and cost. Offshore CO_2 transportation is relatively uncommon with only a couple of examples, including Snøhvit. As a result, offshore pipeline costs vary dramatically with some estimates showing up to a fourteen-fold increase compared to the base onshore case (NETL. 2014), and others showing a much smaller increase of 60-170% (ZEP. 2011b, IEAGHG, 2010). These costs capture the additional material treatment required, compared to onshore pipelines, to reduce corrosion and add weight.

Selecting the appropriate transport method and route is therefore important and considerations have to be made to reduce future permitting time and costs. The cost per tonne of transported CO_2 is most sensitive to utilization rates (IEAGHG, 2010, McCoy and Rubin, 2008 and ZEP. 2011b). The cost can double as a result of halving utilization rate. Delay in bringing sources online can greatly impact the utilization rate. However, if subsequent infrastructure is to be built, underutilization, by oversizing pipelines has a lower

cost than building additional transportation infrastructure (ZEP, 2011b). In effect, integrated networks are able to capture the value in economies of scale, unlike building multiple direct link systems. Many existing pipelines exhibit this, often having spare capacity built in, so higher flow rates can be achieved in future (Vandeginste and Piessens. 2008).

The planning to implementation stage of both offshore and onshore pipelines should take between 4.5-6.5 years, with permitting and ROW issues taking up the majority of the time for onshore pipelines. However, alternate transportation methods provide shorter times to project readiness. For example, an estimated 2-3 years is required to take delivery of a ship (ZEP, 2011b).

2.2.2 Ship Transport

Prior literature predominantly focuses on CO_2 transportation by pipeline. However, ship transport has also gained consideration for the movement of CO_2. Feasibility studies have demonstrated the cost-effectiveness of incorporating shipping along with pipelines for offshore storage. These have included storage off the coast of Japan, capture from cement and ammonia facilities in Norway and shipping with pipeline clusters in Europe (Ozaki et al., 2013, Norwegian Ministry of Petroleum and Energy, 2016, ZEP. 2011b and Roussanaly et al., 2013). The system consists of liquefaction, storage and loading, shipping, and receiving facilities.

For ship transport, it is most efficient to transport the CO_2 as a liquid near its triple point, -56^{o}C and 0.5MPa. The transport capacity of the ship is increased because the CO_2 reaches a density of 1200 kg/m^3 (Rackley, 2010). Additionally, the low pressurization requirements, compared to liquid CO_2 at ambient temperature, reduces the tank thickness requirements (ZEP. 2011b). Liquefaction occurs after the CO_2 stream has been compressed

and heated to a temperature of 50ºC. This reduces the chance of solid CO_2, dry ice, formation during liquefaction (ZEP. 2011b). Once the stream has been liquefied, it is transferred to buffer tanks. This storage allows for a continuous stream of CO_2 from the capture facilities, in spite of the discrete nature of ship transportation. The CO_2 is then transferred to the ships via loading arms.

Ship transport of liquefied gases has been around since the 1940s and falls into three categories (IEAGHG, 2004): pressure type, semi-refrigerated (combined temperature and pressure control), and low temperature. The range of conditions in each of these varies with the properties of the liquid being transported. Liquefied natural gas (LNG) is transported in the low temperature vessels at -164ºC, whereas semi-refrigerated ships are used at around -50ºC for liquefied petroleum gases such as propane and butane (Norwegian Ministry of Petroleum and Energy, 2016, IEAGHG Shipping, ZEP. 2011b). Tradeoffs therefore exist between the temperature and pressure conditions. These can range from a low-pressure scenario (0.6 to 0.8 MPa at -50ºC), which is energy intensive and requires insulation, to high pressure situations (4.5 MPa at 10ºC) which require thick walled tanks.

Table 2. Ship Transport conditions (adapted from Norwegian Ministry of Petroleum and Energy, 2016)

	Semi-Refrigerated	Pressure Type
Temperature	-50°C	10°C
Pressure	0.6-0.8 MPa	~4.5 MPa
Comments	• Energy Intensive • Insulation requirement • Based off LPG semi-ref ships	• Requires more space due to low CO_2 density • Large steel requirement due to tank thickness

Semi-refrigerated ships allow for most flexibility in sizing and possible use as LPG carriers, so reducing the risk of having stranded assets (ZEP. 2011b). It is noted six LPG carriers in Europe, with capacities up to 10,000m^3, are certified to carry CO_2. Specific ship transport of CO_2 also exists, but on a relatively small scale, with four vessels of 1000m^3 each carrying CO_2 at 1.5-2MPa and -30°C (ZEP. 2011b). Hence, the capacity of the proposed ships varies in the literature with two distinct groups: those that suggest sizes in the region of 3000-10,000m^3 (GCCSI, 2011 and Norwegian Ministry of Petroleum and Energy, 2016) and others who use values up to 40,000m^3 (ZEP. 2011b, IEAGHG, 2004, Roussanaly et al. 2013). Unlike pipeline transportation, ship transport provides a non-continuous method of moving CO_2. Therefore, transported capacities are dependent on the size of the ship's tanks, the speed of the ship and the distance to the storage location. Appropriate scheduling of the ships is required to ensure demands are met and that the amount of idle time is reduced. For transportation under 1000km, ship transport is only

weakly related to distance with a stable cost of $10-13/tonne CO_2 (IEAGHG, 2003). This is in contrast to offshore pipelines where cost is directly related to distance.

There are multiple different options for offloading the CO_2, including directly to an injection well, to a platform or storage ship, or to another onshore buffer (Chiyoba and Norwegian Ministry of Petroleum and Energy, 2016). Different options result in different conditioning requirements on the ship. If injecting directly, the ships need the ability to heat and pressurize the CO_2 stream to the required conditions. However, in the other cases these processes can be performed at the specific injection or receiving facility. Direct injection benefits from not needing large offshore facilities, but requires at least one extra ship (Ozaki et al., 2013).

Shipping is beneficial in situations where sources of CO_2 are far from suitable storage reservoirs (Fimbres Weihs et al., 2014, GCCSI, 2011). These benefits are pronounced for long durations due to the fixed costs, associated with liquefaction and dock facilities, becoming a smaller proportion of total costs (IEAGHG, 2004). The loading and unloading times also represent smaller fractions of the total trip time. Hence, for longer journeys the fraction of total transportation time is greater (ZEP. 2011b). Ship transport is shown to be more cost effective than pipeline transport by Fimbres Weihs et al. (2014) for distances over 750km, for a deep offshore pipeline. For transportation between two points that can be reached via waterways or onshore pipeline, this distance increases to 1150km.

Additionally, shipping provides an ideal solution to high-risk, early-stage projects through reducing the chance of stranded assets (ZEP. 2011b and Roussanaly et al., 2013). Ship transport may also be beneficial when small volumes are transported over short distances or there is a ramp up period where the resource isn't fully utilized in the early stages of a project (Mallon et al. 2013 and Ozaki et al. 2013). For projects that don't continue past the demonstration phase, ship transportation provides the benefit of lower

capital costs, 30-50% of annualized costs, compared to 70-90% for pipelines (IEAGHG 2010, ZEP. 2011b, Fimbres Weihs et al., 2014). Additionally, there is the possibility to repurpose the ship for an alternate CCS project or conversion to an LPG carrier, thus providing residual asset value in contrast to pipelines.

For ship transport costs, utilization has the lowest sensitivity leading to the assumption it may be beneficial in projects with large uncertainties and early-stage projects that may pick up significant delays (ZEP. 2011b). Shipping also provides the flexibility to take CO_2 from multiple sources and to switch from one storage site to another. This way the ship is utilized by multiple emitters. The disadvantage of ship transport, for either direct injection or offloading to an offshore site, is the difficulty and expense of scaling it in the future. However, due to the lack of extensive prior experience there are large uncertainties surrounding CO_2 ship transport costs (Norwegian Ministry of Petroleum and Energy, 2016).

2.3 STORAGE

The third sub-system is storage or sequestration. It is estimated the total storage resource in the United States is 8,613 billion tonnes of CO_2, made up of oil and gas reservoirs, un-mineable coal seams and saline formations, the latter making up 96.7% of this total storage capacity (NETL, 2015b). Naturally occurring CO_2 can be found stored within geologic formations. Additionally, CO_2 has been injected into the subsurface for use in CO_2 EOR since the 1970s (IEA, 2013) and injected as part of acid gas disposal since the 1990s (Michael et al., 2010). The suitability of the storage site is dependent on its ability to store CO_2 over geologically significant periods of time, and garner social acceptance, as well as its economic feasibility (Mallon et al. 2013)

The CO_2 can be sequestered geologically via various mechanisms. Initially, the depositional setting, lithology, folds and faults ensure the containment of CO_2 below a low permeability confining system. This is referred to as structural and stratigraphic trapping. Residual trapping occurs due to capillary forces preventing significant percentages of CO_2 from moving from the pore space. Solubility trapping arises when CO_2 dissolves in formation water. Finally, mineral trapping occurs over thousands of years as the carbonic acid, formed through dissolution of the CO_2 in formation water, reacts with minerals (IPCC, 2005 and Bachu, 2003). The time dependent aspects of trapping mechanisms are presented in Figure 7.

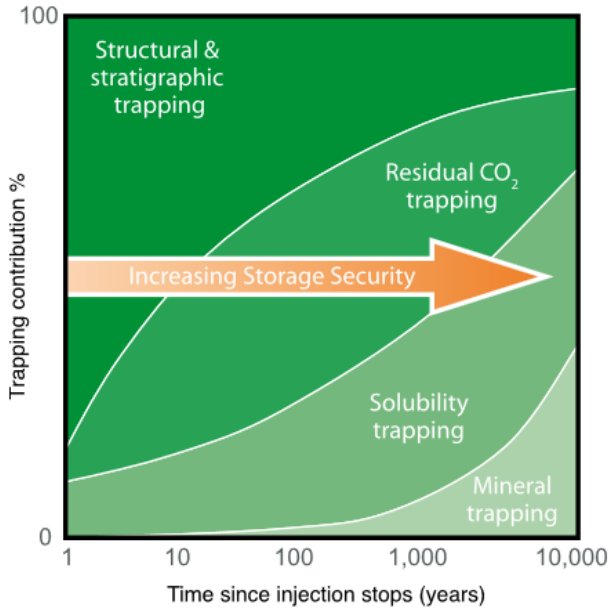

Figure 7. Trapping mechanism contributions as a function of time (IPCC, 2005).

Trapping is vital to the success of the storage reservoir. The ability to reduce the chance of CO_2 leakage from the geologic formation to the atmosphere is one important aspect of the site screening. The lifecycle of a storage site consists of screening,

characterization, permitting, development, commissioning, injection, decommissioning, and monitoring (ZEP, 2011c and NETL, 2014).

In addition to providing a suitable trapping mechanism, the formation must be able to accept the injected CO_2 without overfilling or over pressuring the reservoir. Similar to the characteristics needed for efficient production of hydrocarbons, porosity, formation thickness, and permeability are of particular importance. These characteristics define how much CO_2 can be stored and how quickly it can be injected. Sedimentary basins usually present favorable permeability and porosity conditions; other settings such as basalts and ultramafics have been proposed but the feasibility of large-scale use is less certain (Bachu, 2003).

Tectonic setting is another important characteristic for determining suitability of storage reservoirs, with convergent boundaries being less attractive than divergent ones. Bachu (2003) lists 15 criteria for ranking basins. The ranking provides a suitable way of assessing many basins before conducting a more in-depth characterization. Included in the criteria are reservoir depth and geothermal gradient. These conditions impact the density of the stored CO_2, with higher densities preferred. A greater mass of higher density CO_2 can be sequestered for a given pore volume than lower density CO_2. Additionally, as density increases buoyancy forces are reduced, so reducing the risk of leakage. However, injection into deeper reservoirs increases the drilling costs. Cold basins may be favored, because they give a greater CO_2 density for a given depth (Figure 8). Whether a basin is cold or warm is dependent on the surface temperature and geothermal gradients (Bachu, 2003).

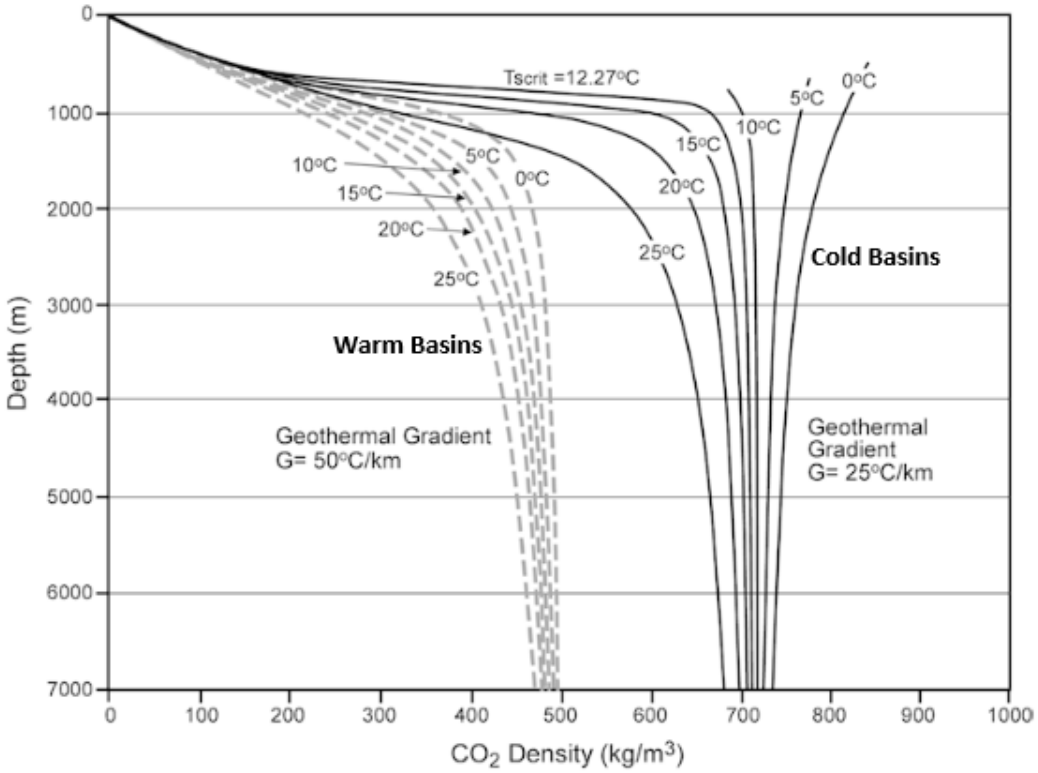

Figure 8. The variation of density with depth for 'cold' and 'warm' basins of various surface temperatures (adapted from Bachu, 2003).

Sensitivity analysis was performed on some of these site-specific factors by ZEP (2011c). The study found that there was a wide range of costs depending on whether the storage was onshore or offshore, if existing wells were used and depending on if the injection occurred into a saline aquifer or depleted oil and gas field. It was found that the cheapest reservoirs, onshore depleted oil and gas fields, contributed least to the total storage capacity. Conversely, offshore saline aquifers provided the greatest capacity, but were the most expensive option at €6-20 per tonne CO_2 stored. Field capacity and injectivity were shown to be two of the most important variables impacting the cost of storage. Sensitivity

to field capacity caused a €10/tonne CO_2 difference in offshore saline aquifers (ZEP, 2011c).

Saline aquifers incur high costs, and time penalties, in part due to the need for exploration. It can take five to ten years to qualify these formations for CO_2 storage (IEA, 2013). However, multiple projects including Sleipner, Snøhvit and In Salah currently utilize such formations for injection. Like oil and gas exploration, there is high uncertainty during exploration and often it is subsequently found that the reservoirs are not suitable (ZEP, 2011c). The total storage capacity in aquifers presents one of the largest uncertainties to whether the CCS goals can be met due to their lack of characterization, with the estimated capacities having an order of magnitude difference (IEAGHG, 2013). The risk for depleted oil and gas fields is much lower as extensive characterization often exists in the form of seismic surveys, well logs, cores and production data. As a result, the exploration costs are expected to be halved. However, these sites will often require a re-evaluation as the mechanics of the reservoir are different during production and injection (IEAGHG, 2009)

Once characterization is complete, permitting and development of the storage site can begin. Depleted oil and gas fields benefit from existing infrastructure. Reutilization of existing wells can reduce the costs significantly. The drilling of wells is one of the largest contributors to a storage site's costs (ZEP, 2011c). Reusing existing wells saves about half the costs of drilling a new well (King et al., 2013) However, suitability for CO_2 injection should be investigated, with measurements to determine corrosion extent and annulus cement integrity (Glazewski, 2016). In the case of the Kingsnorth project, existing wells couldn't be used due to cement and casing integrity issues (Zhou et al., 2014). Wells provide the most likely leakage pathway, so the tradeoff between the costs of making wells suitable for reinjection versus the cost confirming their proper abandonment have to be

considered (ZEP, 2011c). Additionally, existing platforms can often be utilized without needing significant expenditure. It was found that in the proposed Longannet project, the Goldeneye platform could be reused due to its limited production use, having an acid gas rating and ability to be controlled remotely (Zhou et al., 2014).

The next step is injection. During this phase, monitoring, measurement and verification (MMV) of the storage has to be made to ensure the CO_2 is migrating as modeled and there are no leaks. Measurements from the characterization phase can act as a baseline during the subsequent injection. However, there is currently little agreement on what constitutes sufficient MMV. The broad range of technologies, number of measurements and areal extent of measurements can affect the costs dramatically (ZEP, 2011c). These technologies include 4D seismic, microgravity, cross-well electromagnetics, 4D vertical seismic profiling, tracers and numerous geochemical analyses (ZEP, 2011c, Michael et al., 2010 and Chadwick et al., 2005), with some of these methods requiring additional monitoring wells for their deployment. The method, and so the cost incurred, is also largely site specific (Michael et al., 2010), with reservoir size and geologic characteristics affecting the plume migration and so extent of the monitoring required.

The monitoring may continue after the injection has ceased, during the post-injection phase. Once long term, effective, storage has been demonstrated, and models have been validated, in some jurisdictions, responsibility for the site can be transferred. This incurs several costs, including plugging and abandoning all wells not used for post-injection monitoring, and removing any injection facilities and structures (European Commission, 2009). To date, there is limited experience with post-injection monitoring so there are large unknowns regarding monitoring strategies (Michael et al., 2010). There is also no cross-jurisdictional consensus on who retains responsibility and at what point the site can be transferred. In Europe, the post closure period is a minimum of 20 years from

the end of injection operations. For the US, the Underground Injection Control program lists 50 years as the default post-injection monitoring time for CO_2 sequestration, or Class VI, wells. Five states have also passed legislation for transfer of responsibility to the government: Louisiana, North Dakota, Montana, Illinois and Texas (IEA, 2011b). These rules differ from the federal regulations, with liability being passed 30 years after the end of injection in Montana and 10 years in Louisiana. Additionally, Wyoming passed legislation, but in it the responsibility remains attached to the entity who injected it (GCCSI, 2009). In all cases, financial contributions to a liability fund, are required to reduce the financial burden on the state for the monitoring and potential remediation. However, these liability costs vary with €2/tonne CO_2 stored (ZEP, 2011c) and a cap of $5 million for injection in Louisiana (Louisiana House Bill 661, 2009 session).

The regional differences are not merely regulatory. The cost of storing CO_2 in deep saline aquifers was shown to vary between basins, depending on the varying geology and depositional environments, from $9/tonne of CO_2, in the East Texas and Illinois basins, to $22/tonne CO_2 in the Powder River Basin (NETL, 2014).

2.3.1 Enhanced Oil Recovery

Economic benefits can be gained from the subsurface injection of CO_2. These applications include use in enhanced oil, gas or coalbed methane recovery. In these mechanisms, the CO_2 is planned to breakthrough at the producing well to be recycled back to the injection well (Bachu, 2003). The study by ZEP (2011c) excluded enhanced oil recovery for Europe because total storage capacities of saline aquifers were much greater than storage capacities, via tertiary recovery, in oil and gas reservoirs. This is in contrast to NETL (2015a) which presented a future carbon tax scenario, demonstrating, by 2030, 95% of CO_2 sequestration, in the United States, would be via EOR. Unmineable coal seams

were also ignored. Those possessing high gas content may be utilized for CO_2 storage, along with the production of coal bed methane, with such projects existing in Alabama and Virginia (Nemeth, 2006).

Enhanced oil recovery with CO_2 has seen widespread use in the US, with 60 Mt of CO_2 being injected per year (IEA, 2013) and accounting for 6% of US oil production (Kuuskraa et al., 2013). However, only 20% of this is from anthropogenic sources (Kuuskraa et al., 2013). Due to the expense of the CO_2, efforts are made to reduce the amount of CO_2 required per barrel of oil extracted. The permanent storage of the CO_2 is also not of primary importance to the operators, so a different MMV approach is implemented compared to a pure storage project. However, CO_2 EOR projects have the opportunity to lower cost barriers for all CCS projects by driving the development of transportation infrastructure and capture technologies (IEA, 2013). There are numerous ways EOR could be used to stimulate further growth of CCS, including stacked storage. Stacked storage refers to oil bearing formations, where CO_2 EOR can be implemented, which are underlain by saline aquifers. The CO_2 is initially injected into the oil reservoir, before being injected into the saline aquifer as CO_2 use decreases. However, on the longer-term, CCS projects will have to utilize saline reservoirs, with only half of the sources in the south of the US within 250 km of a suitable hydrocarbon formation. The availability of suitable storage formations can impact the overall deployment and ability to meet the emissions reduction goals (IEA, 2013 and IEAGHG 2010).

2.3.2 Offshore Storage

Several current large-scale projects have demonstrated the feasibility of offshore storage, including Sleipner and Snøhvit (CSLF, 2017). Offshore storage has multiple benefits including the abundance of suitable capacity, and public acceptance. It has the

drawback of higher drilling costs, so often seismic is used in MMV to reduce the need for monitoring wells (ZEP, 2011c). Offshore storage also has regulatory uncertainties. The London Protocol controls the dumping of wastes at sea and a provision to allow sub-sea geologic storage of CO_2 was added. However, this does not extend to the export from one country to another for sub-sea geologic storage, therefore limiting the ability of emission reductions, via CCS, in countries without feasible storage locations (Dixon et al. 2014). Cross-border transport will be necessary if the 2^{o}C targets are to be met (IEA, 2013). This pertains specifically to storage rather than for utilization EOR. The amendment proposed to rectify this still needs to be ratified by 29 countries, with only 2 having done so between 2009 and 2014. The London Protocol however does not regulate the disposal of waste if the source is connected to land, in the case of pipelines or via an extended reach well, such as Snøhvit (GCCSI, 2011).

This regulatory uncertainty has the ability to effectively change a country's attitude towards CCS implementation. The wide range of storage options and their associated trade-offs provides no obvious selection for CCS implementation. The combination of the regulatory uncertainty and the broad range of possible storage options presents a situation where optimization can elucidate potentially non-intuitive options.

2.4 OPTIMIZATION

The prior sections demonstrate the wide array of technologies available for CCS implementation. Options within each sub-system feature trade-offs with possibilities for optimization. However, the number of different possible capture, transport and storage options make choosing frontrunners difficult. This paper introduces a model that incorporates many of these factors to generate an optimal CCS network, incorporating sources, sinks, and transportation infrastructure. The optimization seeks to reduce the total

network costs, considering both direct and integrated networks, as well as ship and pipeline transport. By considering multiple options, this mathematical formulation reduces the chance of bias towards a particular solution pathway that can be introduced in qualitative approaches.

Many previous studies have investigated the costs associated with CCS networks, but the majority of these only focused on one or two of the sub-systems (Leung et al., 2014). Fimbres Weihs et al. (2014) compared the economics of ship and pipeline transport, NETL (2014) considered the regional cost variation of transportation and storage and King et al. (2013) proposed bounding capture and storage scenarios, but with a simplified transportation network. Additionally, rudimentary rules are often used to match sources to sink when the system is very large. The investigation by IEAGHG (2010) scored the sources considering the proximity to sinks, terrain and emissions. Up to ten of the closest sources were then selected, whilst ensuring the sink had enough capacity for over 20 years of storage. The result was a global network of both point to point and integrated infrastructure. However, it is a 'greedy' approach where once a source is matched to a sink it can't be considered for any subsequent sinks, thus ignoring many potential cheaper alternatives. A similar method was used by Wenying et al. (2011). The study analyzed point sources and availability of sinks in different regions of China and optimized pipeline routes, utilizing GIS, with attention being placed on protected areas and topographic gradient. The results were compared to an alternate approach, which assessed the cost of matching a source with a sink for all combinations within a search radius. Rockett et al. (2011) performed an analysis for source-sink matching in Brazil. Reservoir analysis was performed and a team of experts in geology and geography then matched sources to sinks. One of the limits of the investigation was the uncertainty surrounding sink capacity. These

results show the wide range of techniques employed in selecting sources and sinks for CCS deployment.

Large sets of feasible alternatives provide difficulties for decisions makers across many different sectors. The prior sections presented the vast array of technologies and potential pathways that CCS development could take. To select optimal solutions from such a vast array of options a methodology is required to aid the decision makers. Multi-criteria decision analysis, MCDA, provides a framework to aid approaching such decision problems (Malczewski, 2006). These frameworks contain an objective with evaluation criteria, decision makers, decision variables, a decision environment and outcomes for each alternative (Malczewski, 2006). Due to the spatial nature of many of the decision problems, MCDA is often combined with geographic information systems, GIS. These decisions consider not only what to do, but where to do it. The utilization of GIS provides important information in the evaluation, but also has results that can easily be interpreted by the decision makers. Multi-criteria decision analysis can be broken up into several subgroups: objective versus attribute based, deterministic versus stochastic, and individual versus group decisions. For attribute based decision problems, there are a discrete set of alternatives that can be individually ranked against evaluation criteria. Objective based decisions have a continuous feasible region of solutions (Malczewski, 2006). Due to the large number of combinations of sources, transportation routes, and sinks, attribute based decision making would be unsuitable for the development of integrated CCS networks.

2.4.1 Decision Analysis

Objective based decision analysis allows for continuous feasible regions to be assessed, with linear-integer programming optimization being most commonly applied method in GIS based problems (Malczewski, 2006). Linear programming presents

problems as a series of linear inequalities, and so generates a feasible region. Depending on whether the aim is to maximize or minimize the outcome, and provided the feasible region is bounded, an optimal value, or values, can be calculated. The matrix formulation of a linear program for minimization is:

$$\min z = c'x \quad (1)$$

$$subject\ to: \quad (2)$$

$$Ax = b, x \geq 0$$

The decision variable is x, with A, b and c representing a matrix and vectors of constants respectively. The value of c'x, is to be minimized in the above equation and is known as the objective function. The constraints on the system are given by Ax = b. Linear programming formulations can be used to solve both deterministic and stochastic problems.

2.4.1.1 Deterministic Models

Linear programming approaches have been widely demonstrated for CCS network optimization (Middleton and Bielicki, 2009; Kuby et al., 2011; Morbee et al., 2011; Han and Lee, 2011; Middleton et al., 2012a, 2012b). All of these approaches utilize mixed integer linear programming, a specific type of linear programming in which decision variables can be restricted to be integers, binary variables or continuous variables. This allows for models to be constructed that capture the significant capital costs and economies of scale seen in CCS projects.

The objective functions of these models minimize the total network cost consisting of the capital and operating costs of the capture, transportation and storage systems. Given

a target value for CO_2 storage, they consider how much to capture at each source, the size and location of pipelines and the amount to inject in each reservoir. The constraints ensure the total storage demand is met, while specifying the amount captured or stored at a node is less than its capacity and ensuring a mass flow balance at each node. The models (Middleton and Bielicki, 2009; Kuby et al., 2011) provide important insights to the reduction of costs of a directed network, compared to direct pipelines. Specifically, as the storage requirement increases so does the cost benefit of an aggregated network over a system that only considers direct pipelines. Han and Lee (2011a) consider scenarios with different carbon credit prices and percentages of electricity demand met by combustion. Their results demonstrate the optimal deployment of generation and emission mitigation strategies, but ultimately show that the maximum benefit is received in situations where the lowest percentage of electricity demand is met via combustion. However, all of these models are static, with only a single decision period, and so do not consider having to build onto an existing network in response to future decision and demand changes.

The design of CCS projects is likely to change over time, reacting to technology changes, new sources and storage locations, as well as changes in policy. The models presented by Morbee et al. (2011) and Middleton et al. (2012b) incorporate this interdependent temporal aspect of building infrastructure. The models balance the benefits of installing infrastructure in an initial period compared to a later one. This addition aims to optimize the phasing in of infrastructure as the system responds to various demands resulting from changes in policy (Middleton et al., 2012b). The research builds on the infrastructure model developed by Middleton and Bielicki (2009). Due to the time dependence of the model, the time value of money is considered. Additional complexity, compared to earlier models, is added with ship transportation and the time availability of reservoirs being considered (Morbee et al., 2011), and bi-directional arcs allowing for flow

direction to change in later time periods (Middleton et al., 2012b). A scenario is presented by Middleton et al. (2012b) for infrastructure build out in Texas over five time periods and 50 years. The results demonstrate the optimal solution overbuilds capacity in earlier time periods, for them to be fully utilized later. In addition, costs are 50% higher, and pipeline lengths are 100% higher, if no foresight is used. The results demonstrate the importance of temporal aspects in creating infrastructure models. However, these models assume perfect knowledge about the future states of the world. In reality, the future demand for CCS is uncertain and so a stochastic implementation is considered in this paper.

2.4.1.2 Stochastic Models

Stochastic programming provides a method for optimizing near term decisions, with the consideration of future uncertainty. Understanding the impacts of the uncertainties, such as future emissions policy, is important in planning infrastructure (Bistline and Weyant, 2013). In stochastic programming, a near term hedging strategy is generated, which provides maximum flexibility across all future scenarios. Once the future state of the world becomes known, recourse action can be taken to adapt the initial solution to the current state. The general formulation for a stochastic model is (Birge and Louveaux, 2011):

$$\min z = c'x + E_{\xi}[q_{\omega}{}'y_{\omega}] \quad (3)$$

$$subject\ to: \quad (4)$$

$$Ax = b,$$

$$T_{\omega}x + W_{\omega}y_{\omega} = h_{\omega},$$

$$x \geq 0, y_{\omega} \geq 0, \forall\ \omega\ \epsilon\ \Omega$$

The values of the coefficient matrix, A, and vectors b and c are known from the outset. However, the terms T_ω, W_ω, h_ω and q_ω are dependent on the state of the world, ω, which has an associated probability p_ω and is drawn from all possible future states of the world Ω. The state of the world, ω, only becomes known after the first-stage decisions are made. The model form is similar to that of the deterministic model but includes additional terms in the objective function and constraints. These terms are dependent on both the first-stage decisions, x, and the second stage decisions y. The additional objective function term represents the expectation of the second-stage value across all realizations of ω (Birge and Louveaux, 2011).

Several metrics can be used to evaluate the value gained by considering the stochastic solution as opposed to a less sophisticated approach (Bistline and Weyant, 2012; Leibowicz, 2018). These include the value of the stochastic solution (VSS) and expected value of perfect information (EVPI). The VSS is used to determine the cost of ignoring uncertainty. It is the difference between a solution which only considers the expected future state of the world (expected value solution), before recourse decisions are made, and that which considers multiple states and their associated probabilities (stochastic solution). To calculate the expected value solution, the problem is deterministically solved using the expected values of uncertain parameters in period two. The first stage solution is then fixed, and the weighted average, considering all recourse actions to adapt to the realized state of the world, is calculated. The expected value solution is a naïve approach: it assumes the future is certain and that this certainty is equivalent to the expected value. The expected value solution was presented by many of the previous papers for dynamic network optimization (Middleton et al., 2012b; Morbee et al., 2011).

The EVPI metric gives a measure of the value of having perfect information before a first stage decision is made. The solutions for each possible state of the world are

optimized deterministically and then averaged. This value is subtracted from the optimal stochastic solution to get EVPI.

Discrete distributions of second stage uncertainties allow the model to be reformulated as an equivalent deterministic model, an approach taken by stochastic programming applications in the energy strategy literature (Han et al. 2012; Bistline and Weyant 2013; Leibowicz 2018). An optimization problem with three possible future states could be re-written as:

$$\min z = c'x + p_1 q_1{}' y_1 + p_2 q_2{}' y_2 + p_3 q_3{}' y_3 \quad (5)$$

$$subject\ to: \quad (6)$$

$$\begin{array}{llll} Ax & & & = b \\ T_1 x + W_1 y_1 & & & = h_1 \\ T_2 x + & W_2 y_2 & & = h_2 \\ T_3 x + & & W_3 y_3 & = h_3 \end{array}$$

$$x \geq 0, y_\omega \geq 0, \forall\, \omega \in \Omega$$

Bistline and Weyant (2013) and Leibowicz (2018) provided examples of how such a stochastic programming methodology could be implemented on different energy problems, and the value in using the VSS and EVPI metrics to assess the results. Han et al. (2012) and Han and Lee (2011b) used discrete uncertainty distributions of emission reductions to model the full-CCS chain in Korea, with the latter including utilization of the CO_2. It was determined that establishing different transportation methods provided the most economical way of adapting to uncertainty, compared to opening new facilities. The results also showed the near term hedging due to the oversizing of pipelines. Disparate results were observed with regards to transportation with Han et al. (2012) showing mainly compressed gas transportation in the most economic case compared to dense phase in Han

and Lee (2011b). Both models demonstrated the utilization of ship transport in stochastic solutions, with this transport mode being shown to provide stability in uncertain environments (Han and Lee 2011b).

Uncertainties can also be modeled as continuous distributions or intervals. Further studies expanded on Han et al. (2012) to show the optimization of carbon capture and storage in Korea with continuous uncertainty distributions. Lee et al. (2017) and Han and Lee (2013) used Monte Carlo simulation to reduce the continuous distributions of operational uncertainties to a manageable set of scenarios, via the Sample Average Approximation method. Multiple objective functions were also considered, with the cost, environmental impact, and either financial or environmental downside (Lee et al. 2017), or technical risk (Han and Lee 2013) being simultaneously minimized. The switch of risk minimization from financial to environment, showed a corresponding change from capture at gas plants to coal plants and a shift in storage formation types. Gas also provided less variation under uncertainty, than coal, due to the lower spread on its input data. Chen et al. (2010) made decisions over three time periods for 10 scenarios, in which multiple parameters were uncertain and defined over an interval. Although the emissions reduction was defined for each scenario, the variation in CCS demand came about from multiple variables such as the uncertainty in power demand and variable CO_2 emissions levels. However, this study only considered three power plants, one coal, one natural gas and one petroleum, without considering the full-chain of CCS.

2.4.2 Network Construction

Many of the previous papers exclude geospatial information in the creation of a network. These papers use a simplified network considering only average distances between regional points (Han and Lee, 2011a, b and 2013; Han et al. 2012; Lee et al.,

2017). Others don't consider transport at all (Chen et al., 2010). Neglecting optimization of the transport infrastructure, and merely using a direct link, has been shown to overestimate pipeline costs by up to 100% (Kuby et al., 2011).

The simCCS and InfraCCS models include route optimization (Middleton and Bielicki, 2009; Kuby et al., 2011; Middleton et al., 2012a, 2012b; Morbee et al., 2011). The potential network is generated using GIS, with a raster cost surface generated via map algebra. The number of factors included in this calculation varies between studies, with only onshore, offshore and mountainous terrain factors included in Morbee et al. (2011) compared to Middleton et al. (2011) that use 30 factors including topography, crossings, ownership, land use, rights of way and population density. The least cost path is then calculated using this weighted cost surface and Dijkstra's algorithm, to connect all possible pairs of sources and sinks. The resulting networks allow aggregation of emissions from multiple sources into a trunk line, which has been shown to demonstrate the economies of scale (Middleton et al., 2012a).

This class of problems is NP-hard, so efforts to reduce the number of nodes and arcs are considered (Middleton et al., 2012a). This is approached in different ways. Sources and sinks are spatially clustered in Morbee et al. (2011) to reduce the network size. A 98-99.5% network reduction was demonstrated by Middleton et al. (2012a) by removing duplicate arcs, collapsing triangles to a centroid and merging nodes within a certain distance.

To date no model has fully integrated the capture, transportation and storage of a CCS network, whilst considering future uncertainties. Additionally, few papers have considered the benefit that less capital-intensive transportation modes may have in uncertain environments.

Chapter 3: Methods

The technological and political uncertainties, previously described, are likely to cause a wide range of future demands for CCS because the stringency of emissions reductions and the methods to achieve these are currently unknown. The model focuses on the demand uncertainty, as it presents a hugely important factor in the development of infrastructure. However, the model could easily be adapted to consider uncertainty surrounding other aspects of CCS.

Previous studies list the importance of building flexible networks that consider both short and long-term CCS objectives (IEAGHG, 2010). The IEA (2013) lists a key action as encouraging efficient infrastructure development through consideration of future CCS demands. To date, numerous models for optimal CCS infrastructure development have been developed. However, these solutions have either excluded the temporal, spatial or uncertainty aspects that are inherent to CCS projects. The aim of this study is to develop a model that considers all three to generate an integrated capture, transportation and storage network for CCS.

The model can be thought of as being split into multiple steps including the pre-processing of data, network generation, post-processing and optimization:

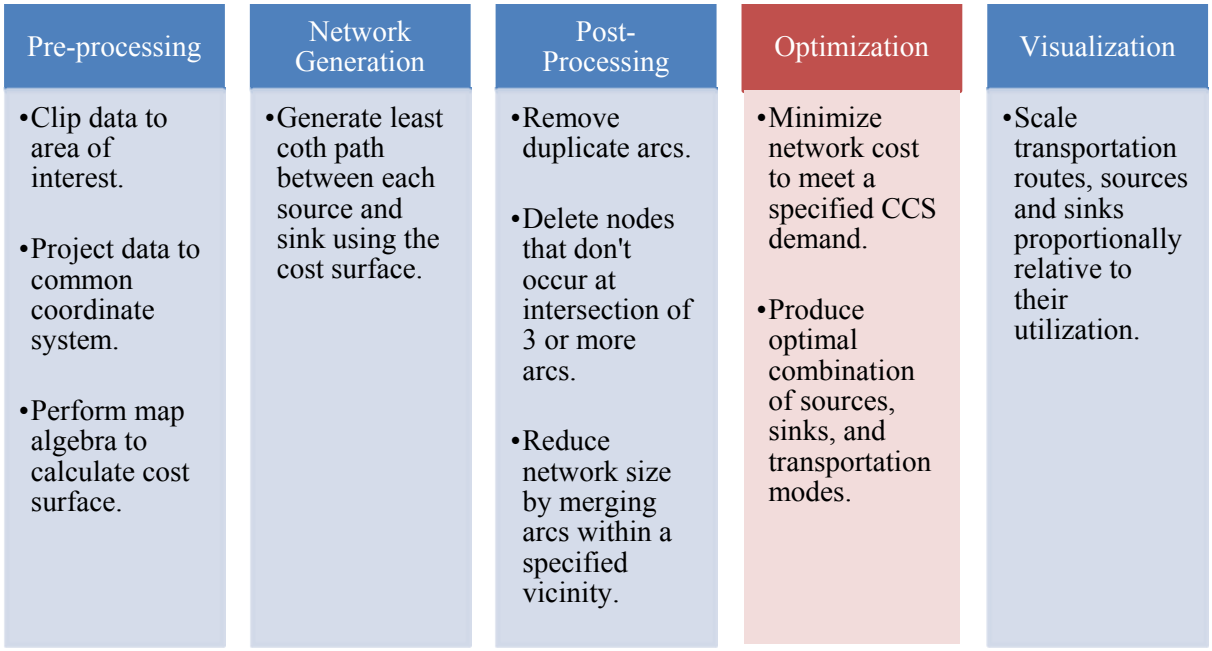

Figure 9. The generalized steps in the model and descriptions, with those in blue performed in GIS and the orange step using the CPLEX solver.

3.1 Geographic Information Systems

It aims to simplify the user involvement, by only requiring information on sources, storage locations and future CCS demands. Three comma separated variable files must be filled out by the user before the analysis can take place, Table 3.

Table 3. Inputs parameters required for analysis

Sources	**Sinks**	**Demand**
Latitude	Latitude	CCS Demand Period 1
Longitude	Longitude	CCS Demands Period 2
Capital Cost	Capital Cost	Demand Probabilities Period 2
Fixed O&M	Fixed O&M	
Variable O&M	Variable O&M	
Emissions Rate	Total Capacity	
Availability in Period 1	Well Injection Rate	
	Fixed Well Cost	

Due to the geospatial aspect of the optimization, GIS was selected as the interface for the model. This allows the interactive selection of the area of interest along with the specification of the network resolution. These parameters should be considered together, with larger analysis areas requiring larger cell sizes in order to maintain a reasonable completion time.

The model must construct a transport network consisting of nodes and arcs between each source and sink, along with calculating their corresponding costs. Previous studies have provided methods of generating this optimized network, with varying numbers of input parameters (NETL, 2006; Morbee et al., 2011; Middleton et al., 2012a). A variation on the construction cost factor presented by NETL (2006) was used. This incorporates eight factors which represent the cost for a pipeline to traverse a cell that includes certain features, Table 4. If a particular feature or topography falls within a certain cell, then the sum of the cost factors for present features is calculated. The optimization algorithm tries to avoid cells with higher costs in order to generate the route with the lowest total cost.

Additionally, offshore pipeline cell values are multiplied by two, to represent the premium over the onshore base case (ZEP, 2011b).

Table 4. Relative construction cost factors and the data sources (NETL, 2006).

Parameter	**Weighting**	**Source**
Base Case	1	-
Slope: 10-20%	0.1	
Slope: 20-30%	0.4	USGS (2017)
Slope: >30%	0.8	
Populated Area	15	USEPA and USGS (2012);
Wetland	15	Homer et al. (2015)
National Park	30	NPS (2017)
State Park (Texas Only)	15	TPWD (2016)
Waterway Crossing	10	USEPA and USGS (2012); Homer et al. (2015)
Railroad Crossing	3	USDOT (2017)
Highway Crossing	3	U.S. Census Bureau (2015)

3.1.1 Pre-Processing

The model consists of a geodatabase, which organizes multiple spatial data into one location. It contains data for each of the parameters in Table 4 for the whole of the contiguous United States, with the exception of State Parks. Due to the size of the datasets, the initial step of the preprocessing clips them to the user-defined extent.

These data exist in either vector or raster format and can have numerous different projections. Rasters are made up of grid cells, with each cell having a certain value. Both USGS (2017) and Homer et al. (2015) are raster datasets. These layers are reclassified to match the weightings in Table 4 and resampled to the cell size defined during initialization. The remaining datasets are vector files. Pipelines are removed from USEPA and USGS (2012) as existing rights of way can have a positive impact on overall transportation costs (Serpa et al., 2011). The vector datasets are then converted to rasters and classified according to Table 4. All of the datasets are subsequently projected to a common, user-defined coordinate system, so that the cells overlie each other. The cost surface is simply generated by adding all of the layers together using map algebra.

3.1.2 Network Generation

The cost surface from the pre-processing step is used to iteratively generate the least cost path between each source node and sink node, via Dijkstra's algorithm (1959). The output is a series of raster files, with each file containing the least cost path from each sink to all of the sources. Often, multiple routes share common sections along their least cost path. These sections are automatically combined, creating a trunk line. All of the raster files are converted to vector format and merged, resulting in one large network joining all of the sources and sinks.

3.1.2.1 Shipping Network

At the time of initialization, the user is given the opportunity to include barge transportation in the analysis. This is potentially useful in uncertain scenarios, associated with early stage projects, where offshore storage is available (ZEP. 2011b; Mallon et al. 2013; Ozaki et al., 2013; Roussanaly et al., 2013 and Han and Lee, 2011b). A similar

methodology to the pipeline network generation is used. However, a second cost surface is utilized, which now includes shipping routes (U.S. Army Corps of Engineers, 2018). These paths are given an arbitrarily low weighting, to force the model to calculate the shortest path from each source to the available waterway. The resulting least cost path's land portion represents the optimal pipeline route to a port. The costs for both the pipeline and shipping sectors are then computed. The shipping costs are constant across all possible routes, as it was shown there is only a weak dependence on distance for lengths less than 1000 km (IEAGHG, 2004). The pipe to the dock and subsequent ship transport are considered as a single transportation arc. Combining the pipe arc to the shipping arc showed significantly reduced solution times, compared to a scenario in which they were considered by optimization separately. To ensure computational feasibility, it is also assumed that the ships can only serve as direct links between a single source and single sink. The combined network often contains extraneous nodes and arcs. The optimization problem is NP-hard, so removal of unnecessary network features can have significant time savings (Middleton et al., 2012a).

3.1.3 Post-Processing

The network is initially separated into arcs that occur onshore versus those that are offshore. This allows two additional steps to be performed on the offshore pipelines. Firstly, a cost multiplier can be applied to these arcs (ZEP, 2011b). Also, it allows this network to be simplified due to fewer routing restrictions. A similar simplification is also applied to the onshore arcs: duplicate arcs are deleted and those falling within a certain distance of each other are made coincident. Once this analysis is complete, the onshore and offshore networks are recombined. Intermediate nodes are then generated at vertices where three or more arcs join.

The intermediate nodes, along with the sources and sinks, are compiled into a table and assigned unique identifiers. The 'Start Node' and 'End Node' are assigned to each arc in the network using these identifiers. Costs for different pipe diameters are then calculated for each arc. The fixed costs are determined using the modified MIT equation from Essandoh-Yeddu and Gülen (2009) and escalation factors from the Oil and Gas Journal data, whilst variable costs are calculated, on a per tonne of CO_2 transported basis, given the pressure drop along the length of an arc. These pumping costs would be incurred at the capture site, but are dependent on factors including the length of the pipe. Further information on cost calculations can be found in Appendix B.

The arc and node tables for the pipeline and shipping routes are exported to an Excel file and a Python script is used to launch the optimization program.

3.2 OPTIMIZATION

The minimum cost network problem was formulated as a mixed-integer program (MIP), which was solved by a CPLEX optimizer. The objective is to decrease the total system costs, whilst meeting a total CCS demand and considering uncertainty regarding the future need for CCS. The outcome is a network that can be implemented now, which provides the minimum cost, and maximum flexibility, to adjust to all possible future states of the world.

The decision variables are made up of continuous, integer and binary values. The continuous values include the amount of CO_2 to capture or store at each point, depending on whether it is a source or sink. Additionally, the amount of CO_2 transported along a given arc is also computed. The majority of the decision variables are integer values and consider the number of pipelines, of a given diameter, to build and operate between sets of nodes, the number of ships to build, as well as the number of wells to drill in a reservoir. For each

of these, the decision in period two considers the infrastructure existing from period 1. The decision becomes how many of each to operate and therefore how many more are needed to be built. In the case of ships, they can also be sold for a depreciated value. Finally, binary values indicate whether or not to open capture and storage facilities in a given period.

The model utilizes some of the structure from simCCS, adding additional transportation modes as well as considering uncertainty (Middleton and Bielicki, 2009).

$$Minimize \quad Total\ Cost \tag{7}$$

$$= \sum_{i \in N} \left(VS_i a_{i11} + FS_i c_{i11} + OS_i h_{i11}^S + VR_i b_{i11} + FR_i d_{i11} + OR_i h_{i11}^R + FW_i w_{i11} \right)$$

$$+ \sum_{m \in M} \sum_{d \in D} \left(FP_{md} g_{md11} + OP_{md} y_{md11} \right)$$

$$+ \sum_{(i,j) \in M} \left(VP_{ij} x_{ij11} \right)$$

$$+ \sum_{(i,j) \epsilon L} \left(VBs_{ij11} \right)$$

$$+ \sum_{l \epsilon L} \left(FBk_{l11} + OBv_{l11} \right)$$

$$+ z \sum_{\omega \epsilon \Omega} p_\omega \left(\sum_{i \in N} \left(VS_i a_{i2\omega} + FS_i c_{i2\omega} + OS_i h_{i2\omega}^S + VR_i b_{i2\omega} + FR_i d_{i2\omega} + OR_i h_{i2\omega}^R + FW_i w_{i2\omega} \right) \right.$$

$$+ \sum_{m \in M} \sum_{d \in D} \left(FP_{md} g_{md2\omega} + OP_{md} y_{md2\omega} \right)$$

$$+ \sum_{(i,j) \in M} \left(VP_{ij} x_{ij2\omega} \right)$$

$$+ \sum_{(i,j) \in L} \left(VBs_{ij2\omega} \right)$$

$$\left. + \sum_{l \epsilon L} \left(FBk_{l2\omega} + OBv_{l2\omega} - DVf_{l2\omega} \right) \right)$$

Subject To:

$$\sum_{i \in N} b_{it\omega} = T_{t\omega} \qquad \forall t \in T, \forall \omega \in \Omega_t \qquad (8)$$

$$a_{it\omega} \leq A_{it} Q_i^S h_{it\omega}^S \qquad \forall i \in N, \forall t \in T, \forall \omega \in \Omega_t \qquad (9)$$

$$b_{it\omega} \leq Q_i^R h_{it\omega}^R - b_{i(t-1)\omega} \qquad \forall i \in N, \forall t \in T, \forall \omega \in \Omega_t \qquad (10)$$

$$b_{it\omega} \leq Q_i^W \sum_{\tau=t-1}^{t} w_{it\omega} \qquad \forall i \in N, \forall t \in T, \forall \omega \in \Omega_t \qquad (11)$$

$$c_{it\omega} = h_{it\omega}^S - h_{i(t-1)\omega}^S \qquad \forall i \in N, \forall t \in T, \forall \omega \in \Omega_t \qquad (12)$$

$$d_{it\omega} = h_{it\omega}^R - h_{i(t-1)\omega}^R \qquad \forall i \in N, \forall t \in T, \forall \omega \in \Omega_t \qquad (13)$$

$$\sum_{j \in N_i} (x_{ijt\omega} + s_{ijt\omega}) - \sum_{j \in N_i} (x_{jit\omega} + s_{jit\omega}) = a_{it\omega} + b_{it\omega} \qquad \forall i \in N, \forall t \in T, \forall \omega \in \Omega_t \qquad (14)$$

$$x_{ijt\omega} \leq \sum_{d \in D} y_{ijdt\omega} Q_{ijd}^{PU} \qquad \forall i \in N, \forall j \in N_i, \forall t \in T, \forall \omega \in \Omega_t \qquad (15)$$

$$x_{ijt\omega} \geq \sum_{d \in D} y_{ijdt\omega} Q_{ijd}^{PL} \qquad \forall i \in N, \forall j \in N_i, \forall t \in T, \forall \omega \in \Omega_t \qquad (16)$$

$$g_{mdt\omega} = \begin{cases} y_{ijdt\omega} - y_{ijd(t-1)\omega}, & y_{idt\omega} - y_{ijd(t-1)\omega} > 0 \\ 0 \end{cases} \qquad \forall m \in M, \forall ij \in N_m, \forall d \in D, \forall t \in T, \forall \omega \in \Omega_t \qquad (17)$$

$$s_{ijt\omega} \leq v_{lt\omega} Q^B \qquad \forall l \in L, \forall ij \in N_l, \forall t \in T, \forall \omega \in \Omega_t \qquad (18)$$

$$k_{lt\omega} = \begin{cases} v_{lt\omega} - v_{l(t-1)\omega}, & v_{lt\omega} - v_{l(t-1)\omega} > 0 \\ 0 \end{cases} \qquad \forall l \in L, \forall t \in T, \forall \omega \in \Omega_t \qquad (19)$$

$$f_{lt\omega} = \begin{cases} 0, & v_{lt\omega} - v_{l(t-1)\omega} > 0 \\ v_{lt\omega} - v_{l(t-1)\omega} \end{cases} \qquad \forall l \in L, \forall t \in T, \forall \omega \in \Omega_t \qquad (20)$$

$$a_{it\omega} \geq 0 \qquad \forall i \in N, \forall t \in T, \forall \omega \in \Omega_t$$

$$b_{it\omega} \geq 0 \qquad \forall i \in N, \forall t \in T, \forall \omega \in \Omega_t$$

$$c_{it\omega} \in 0, 1 \qquad \forall i \in N, \forall t \in T, \forall \omega \in \Omega_t$$

$$d_{it\omega} \in 0, 1 \qquad \forall i \in N, \forall t \in T, \forall \omega \in \Omega_t$$

$$f_{lt\omega} \in 0, 1, 2 \qquad \forall i \in N, \forall t \in T, \forall \omega \in \Omega_t$$

$$g_{mdt\omega} \in 0, 1 \qquad \forall m \in M, \forall d \in D, \forall t \in T, \forall \omega \in \Omega_t$$

$$k_{lt\omega} \in 0, 1, 2 \qquad \forall i \in N, \forall t \in T, \forall \omega \in \Omega_t$$

$$s_{ijt\omega} \geq 0 \qquad \forall ij \in N_l, \forall t \in T, \forall \omega \in \Omega_t$$

$$v_{lt\omega} \in 0, 1, 2 \qquad \forall i \in N, \forall t \in T, \forall \omega \in \Omega_t$$

$$w_{it\omega} \in 0, 1, 2, 3 \qquad \forall i \in N, \forall t \in T, \forall \omega \in \Omega_t$$

$$x_{ijt\omega} \geq 0 \qquad \forall i \in N, \forall j \in N_i, \forall t \in T, \forall \omega \in \Omega_t$$

$$y_{mdt\omega} \geq 0 \qquad \forall m \in M, \forall d \in D, \forall t \in T, \forall \omega \in \Omega_t$$

Table 5. Model decision variables

Decision Variable	
$\boldsymbol{a_{it\omega}}$	amount of CO_2 captured at node *i*, in time *t* and in realization *ω,* in tCO_2
$\boldsymbol{b_{it\omega}}$	amount of CO_2 stored at node *i*, in time *t* and in realization, *ω* in tCO_2
$\boldsymbol{c_{it\omega}}$	0 or 1 depending on whether a capture facility is installed at node *i*, in time *t* and in realization *ω*
$\boldsymbol{d_{it\omega}}$	0 or 1 depending on whether a storage facility is installed at node *i*, in time *t* and in realization *ω*
$\boldsymbol{f_{lt\omega}}$	number of ships sold at depreciated value in time *t* and in realization *ω*
$\boldsymbol{g_{mdt\omega}}$	number of pipelines, of a given diameter *d*, build along arc *m,* in time *t* and in realization *ω*
$\boldsymbol{h^R_{it\omega}}$, $\boldsymbol{h^S_{it\omega}}$	0 or 1 depending on whether the reservoir(R) or source(S) is currently open in time *t* and in
$\boldsymbol{k_{lt\omega}}$	number of ships bought, for transport along arc *l,* in time *t* and in realization *ω*
$\boldsymbol{s_{ijt\omega}}$	amount of CO_2 transported from node *i* to node *j,* by ship, in time *t* and in realization, *ω* in tCO_2
$\boldsymbol{v_{lt\omega}}$	the number of ships that are currently operational, in time *t* and in realization *ω,* for transportation along arc *l*
$\boldsymbol{w_{it\omega}}$	number of wells drilled at node *i,* in time *t* and in realization *ω*
$\boldsymbol{x_{ijt\omega}}$	amount of CO_2 transported from node *i* to node *j,* by pipeline, in time *t* and in realization, *ω* in tCO_2
$\boldsymbol{y_{mdt\omega}}$	the number of pipelines of diameter *d*, from node *i* to node *j* that are currently open in time *t* and in realization *ω*

Table 6. Model Inputs

Inputs	
$\boldsymbol{T_{t\omega}}$	Total mass of CO_2 to be stored in time t and state of the world, **ω.**
$\boldsymbol{FB, FP_{md}, FR_i\ FS_i, FW_i}$	Capital cost for building a ship, constructing a pipe of diameter *d* on arc *m,* opening a reservoir at node *i,* opening a source at node *i,* or constructing a well at node *i.* The pipeline and ship capital costs are an output of the GIS model.
$\boldsymbol{OB, OP_{md}, OR_i\ OS_i}$	Fixed operating cost for a ship, pipe of diameter d on arc m, reservoir at node i, or source at node i. The fixed pipeline and shipping costs are an output of the GIS model.
$\boldsymbol{VB, VP_{ij}, VR_i\ VS_i}$	Variable operating costs a ship, pipeline between nodes *i* and *j,* reservoir at node *i,* and source at node *i.* The variable pipeline and shipping costs are an output of the GIS model.
$\boldsymbol{Q^B, Q^{PL}_{ijd}, Q^{PU}_{ijd}, Q^R_i, Q^S_i, Q^W_i}$	Ship capacity, lower flow rate for a pipe diameter *d* between nodes *i* and *j,* capacity at node *i*, emissions rate at node *i,* and the maximum injection rate of $\boldsymbol{a}$ well at node *i.* These rates are computed over the length of the time period.
$\boldsymbol{DV}$	The depreciated value of the ship, using straight line depreciation.
$\boldsymbol{A_{it}}$	Availability of node *i* to implement capture in time *t.*
$\boldsymbol{p_\omega}$	Probability of state of the world, *ω*, occurring.
$\boldsymbol{z}$	Period two discount factor.

Table 7. Sets used in model

Sets	
$\boldsymbol{T}$	Set of time periods
$\boldsymbol{D}$	Set of all pipeline diameters
$\boldsymbol{M}$	Set of all pipeline arcs
$\boldsymbol{L}$	Set of all shipping routes
$\boldsymbol{N, N_i, N_l, N_m}$	Set of all nodes, nodes adjacent to node *i*, nodes in arc *l,* and nodes in arc *m*
$\boldsymbol{\Omega_t}$	Set of states of the world in time *t*. When *t* is one, there is only one possible state of the world.

The objective value, (7), is split into the first stage costs and second stage costs to demonstrate the impact each set of decisions has on the overall cost. The objective function consists of the capital and operating costs for opening and operating a source, pipeline, ship, storage reservoir and wells. The future costs are multiplied by the probability of each realization and summed to get the expected second-stage value. The second-stage allows for any ship purchased in the first stage to be sold. Only ships were assumed to have residual value (ZEP, 2011b), as they can be mobilized for other CCS projects or used as LPG carriers. Straight line depreciation, using the length of one time period, was used to calculate this value. A discount factor, z, is included as a multiplier, to allow some flexibility within the model. To discount the future costs back to present value:

$$z = \frac{1}{(1+r)^{\tau-1}} \tag{21}$$

Where r is the discount rate and τ is the length of a time period. However, z can be set to values greater than one if it is desired to penalize delays of action.

The total demand for CCS must be met via geologic storage (8). If a source is open, the CO_2 can be captured up to its total emissions' rate for the period (9). An availability factor is used so that proposed sources can be limited to come online in the latter time period, which allows flexibility to consider facilities that are currently under construction or in the pre-financial investment decision phase. For CO_2 to be injected in a reservoir, it must be open and have remaining storage capacity (total capacity minus prior injection) shown by equation (10). It is also restricted by the number of wells and the corresponding injection rates (11). The fixed costs of both capture and storage are dependent on the number of facilities built and operating in a certain period. The number of facilities that are built is calculated by subtracting those operating in the preceding time period from the number of facilities operating in the current period (12, 13). Additionally, the number of pipelines and barges built in a given period is calculated (17, 18). The model also allows for pipelines to be closed and for ships to be sold (19).

The capacity of a ship dictates the maximum volume of CO_2 that can be transported (18). Upper and lower limits constrain the flow in the pipeline network (15, 16). The upper flow limit for each diameter is determined via the set of equations by Vandeginste and Piessens (2008) assuming a maximum pressure drop of 49 Pa/m (NETL, 2006), see Appendix C. This pressure drop ensures the CO_2 remains in the dense phase, whilst also staying below the maximum operating pressure of the pipeline. The upper flow limits are calculated during the analysis in GIS. The lower limit is set to 0 (Middleton et al., 2012a), but the model provides flexibility to adjust this value. A mass balance is performed at every node in the network, balancing the flows into and out of a node with any additions or removals of CO_2 from the network via capture and storage respectively (14).

The Excel files produced during the post-processing stage in GIS are used as the inputs into the model. Once the optimization has completed, the decision variables are then output to a similar set of Excel files.

3.3 VISUALIZATION

These decisions variables are imported into the GIS software. All of the node sizes are scaled proportionally, corresponding to the attributable mass of CO_2 captured, transported or stored during time period t and for a state of the world ω.

Chapter 4: Case Study

Nearshore and offshore of East Texas and the Gulf Coast of the USA was chosen to demonstrate the methodology, as the region presents a favorable area for long-term storage, due to the large number of extensive, permeable, porous sandstone bodies, and suitable seals in the form of shale beds (Treviño and Meckel, 2017). Additionally, the region has numerous CO_2 industrial point sources. These include high purity CO_2 sources such as hydrogen, ammonia, and ethylene oxide production facilities. The model considered 12 industrial sources of CO_2 emissions and 5 selected example reservoirs. The potential of each of the sources is dependent on the technologies employed at each site. However, the data pertaining to different sources are not readily available (IEA, 2011a). Therefore, an extensive review of industrial sources was carried out to determine emissions volume from each, along with the associated processes and any implementation of CO_2 capture technology.

4.1 Source Data

This region has extensive experience with oil and gas exploration and as a result has developed petrochemical and natural gas processing industries. Data were gathered on 248 sources in the study area, stretching from Galveston County, Texas, to Cameron Parish, Louisiana. The EPA's Greenhouse Gas Reporting Program (40 CFR Part 98) requires facilities that emit over 25,000 tonnes CO_2e to report their emissions. The emissions are attributed to 41 categories depending on the responsible processes. Code was developed to gather data from each of the EPA reports. These included total emissions, historic emissions, emissions by chemical process, location and ownership.

Sources were assessed on the emissions from certain categories related to high purity CO_2 streams. Of particular interest were the emissions from hydrogen production,

ammonia manufacturing, ethanol production, petrochemical production, and petroleum and natural gas systems. Categories such as petrochemical production include a wide range of processes, so further refinement was added by searching for phrases relating to specific processes like ‘ethylene oxide production’ or ‘acid gas removal’.

In addition, industry publications were used to determine proposed high purity sources for the region. These included a methanol production facility, two hydrogen producers and three LNG exporters. These proposed sources were assessed on estimated completion date and the approximate emissions from their environmental impact reports. The approximate emissions provide another source of uncertainty. The emissions from CO_2 removal at LNG export facilities assumes a worst-case scenario in which the pipeline gas is delivered at its upper CO_2 limit of 2% by volume. However, local natural gas composition profiles suggest the delivered gas would contain lower levels of CO_2, from 0.6-1.7% by volume (TCEQ, 2012). For the purpose of the simulation, it was assumed the data in the assessments provided a reasonable estimation for future emissions. The model incorporates sources that are still in the planning phases. Therefore, to allow the network to be optimized considering the future location of CO_2 emitters, an availability parameter was set to exclude these sources from the first stage solution. This ensures that sources can only be integrated into the network after their completion date, once they are fully operational.

Twenty-four high purity sources were then selected to be further assessed. A detailed process determination was carried out for each, with TCEQ and FERC filings used to determine specific processes carried out at each facility. Twelve sources were then selected for the study based on the magnitude of the emissions stream and vicinity to La Porte and Port Arthur. These are summarized in Table 8.

Table 8. Selected High Purity CO_2 Emissions Sources

Source Name	**High Purity Emissions Stream, tCO_2 per annum**	**Capture Technology**	**Available for Capture in Period 1**
Praxair Port Arthur #379	1,014,000	PSA	Yes
Praxair Port Arthur Facility	721,000	PSA	Yes
Praxair Texas City Hydrogen Complex	1,402,000	MDEA	Yes
Linde Gas North America LLC, La Porte Plant	1,135,000	Rectisol	Yes
American Air Liquide, La Porte	691,000	PSA	Yes
Linde Gas North America LLC, Clearlake Plant	601,000	Rectisol	Yes
Air Liquide Large Industries US	575,000	PSA	Yes
Air Products Pasadena	501,000	PSA	Yes
Port Arthur LNG	887,000	MDEA	No
Sabine Pass LNG	1,484,000	MDEA	Yes
Golden Pass LNG	1,125,000	MDEA	No
Huntsman Petrochemical LLC, Port Neches Performance Products	220,000	Potassium Hydroxide	Yes

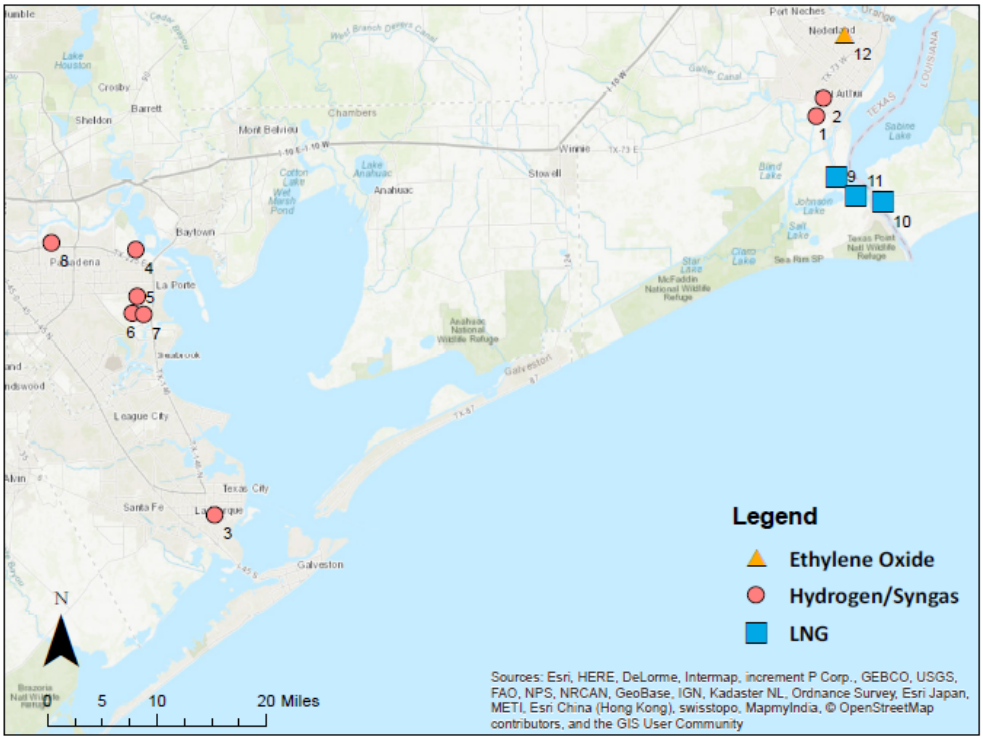

ID	Name
1	PRAXAIR PORT ARTHUR #379
2	PRAXAIR PORT ARTHUR FACILITY
3	PRAXAIR TEXAS CITY HYDROGEN COMPLEX
4	LINDE GAS NORTH AMERICA LLC, LA PORTE PLANT
5	LA PORTE STEAM METHANE REFORMER (AMERICAN AIR LIQUIDE)
6	LINDE GAS NORTH AMERICA LLC, CLEARLAKE PLANT
7	AIR LIQUIDE LARGE INDUSTRIES US - SMR
8	AIR PRODUCTS LLC - PASADENA SMR
9	PORT ARTHUR LNG
10	SABINE PASS LNG
11	GOLDEN PASS LNG
12	HUNTSMAN PETROCHEMICAL LLC PORT NECHES PERFORMANCE PRODUCTS

Figure 10. A map of the source locations, and types, considered in the case study

4.2 Reservoir Data

The Gulf Coast region also presents a favorable area for storage. Oil and gas development has taken place here for over 70 years, thus there are numerous subsurface characterization data available (Carr et al., 2016; Treviño and Meckel, 2017). However, for this study EOR won't be considered, with the optimization focusing on storage.

The Lower Miocene interval has been characterized at depths of 3,000-10,000 feet for offshore CO_2 storage. Multiple porous and permeable sandstones overlay each other, which presents an opportunity for stacked storage development (Meckel et al., 2017). These formations have porosities and permeabilities averaging 28.2% and 338 mD respectively (Seni et al., 1997). Seals within the Miocene interval isolate the stacked storage zones and are over 400 feet thick in the majority of places (Meckel et al., 2017). This shale is identified by the benthic foraminifera Ampistegina chipolensis (Amph. B). Due to the extensive characterization of the area, confidence in the availability of suitable storage is high.

For this study, five representative locations were selected. Various data sources were integrated over the field delineations, in GIS, to approximate reservoir properties. Several factors were determined including the number of wells in a given field, the depth to the top of the Lower Miocene and the areal extent. These data were obtained from a variety of sources including the NATCARB database (NETL, 2015b) and CO_2 brine database (GCCC, 2013). An approximation to the total storage capacity was determined using data presented by Carr et al. (2016). Table 9 presents the fields and their properties.

Table 9. Selected Storage Locations

Field Name	Capacity, $MtCO_2$	Area, km^2	Well Count	Field Control	Depth to top Lower Miocene, m
HIGH IS BK 24-L	28	11.35	32	State	1524
HIGH IS BK10L G	25	4.38	13	State	1828
GA255	51	13.28	8	Federal	2438
HI111	20	22.28	22	Federal	2133
SA010	8	15.95	10	Federal	2438

The locations of the selected case study fields are shown in Figure 11.

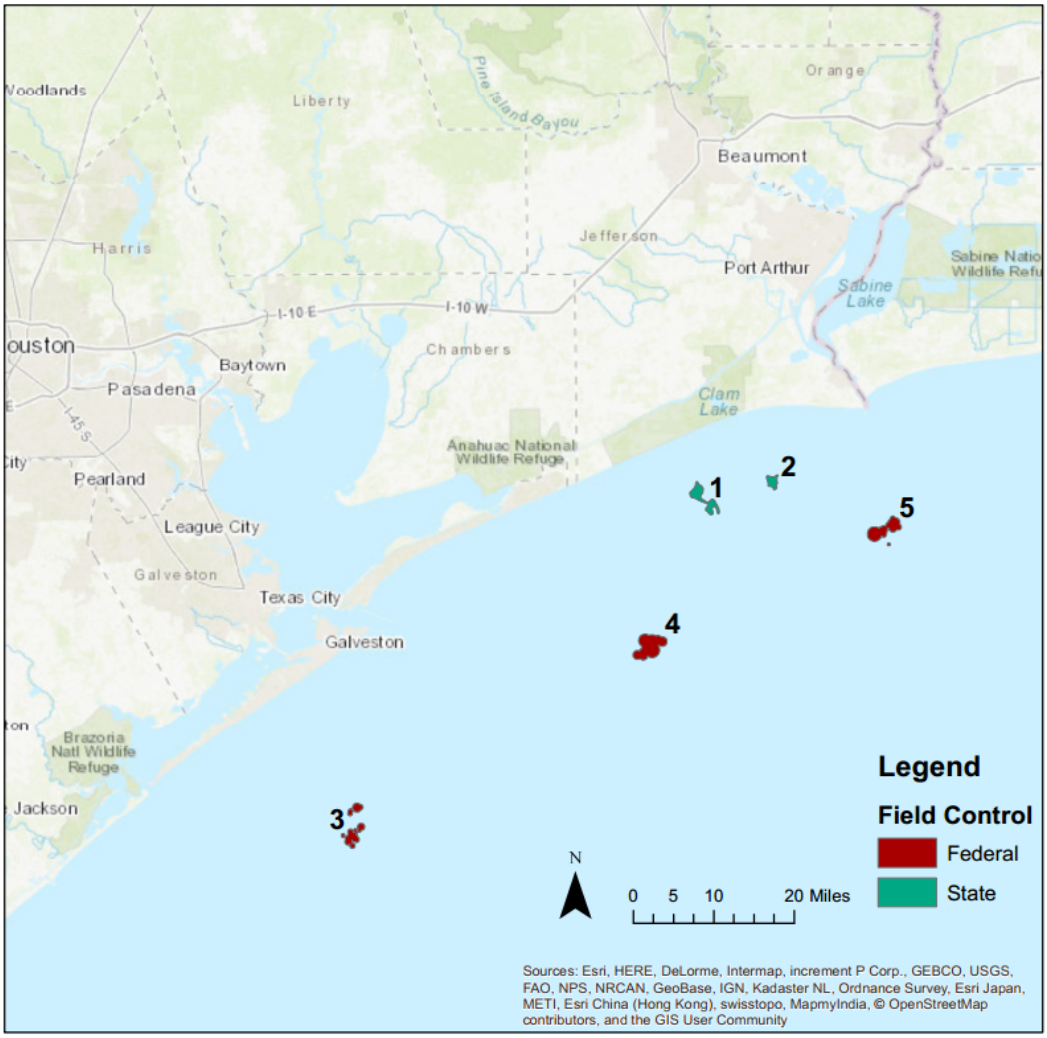

ID	Field Name	Area, sq. km	Field Control
1	HIGH IS BK 24-L	11.35	State
2	HIGH IS BK10L G	4.38	State
3	GA255	13.28	Federal
4	HI111	22.28	Federal
5	SA010	15.95	Federal

Figure 11. The locations of the fields used in the study

4.3 Cost Calculations

After sources and reservoirs had been selected, costs specific to each site had to be calculated. Studies to date have tended to focus on the costs associated with one subsystem

of the CCS chain. An extensive literature review was used to compile a suite of formulae that could be used to calculate costs for each source, reservoir and transportation mode. The costs considered for each subsystem are shown in Table 10. A complete listing of the equations used to calculate each of the listed costs is included in Appendix B.

Table 10. The costs considered in the analysis of each subsystem

	Capital Costs	**Fixed O&M**	**Variable O&M**
Capture	- Capture Plant - Compressor - Pump	- Maintenance - Chemicals - Catalysts - Labor - Fixed Energy Penalty (for retrofit plants)	- Pump Energy Requirement - Compressor Energy Requirement
Transportation	- Pipeline - Ship - Liquefaction - Loading Arms - Buffer Storage	- Maintenance - Fuel - Labor	- Pump Energy Requirement - Harbor Fee - Liquefaction Energy and Water Requirement
Storage	- Drilling Equipment - Well Equipment - Permitting - Injection Test - Post Injection Monitoring - Decommissioning - MMV - Seismic - Contingency	- Maintenance - Seismic	- Liability Fund

4.3.1 Capture Costs

The capture costs generally represent the largest percentage of the full chain CCS costs (ZEP, 2011a). However, by using facilities that had high purity streams of CO_2 available in the case study, these costs were reduced. The detailed analysis of each source allowed the determination of whether additional capture plant were required. All of the facilities that implemented pressure swing absorption required additional capture due to low concentration of CO_2 in the tail gas: 45-50%. Costs were scaled from IEAGHG (2017) which presented multiple options for fitting capture technology to steam methane reformers. Although it was shown not to be the cheapest option, the costs for the scenario in which capture occurred on the PSA tail gas were used. This represents the most likely scenario for retrofitting existing hydrogen production facilities. Compression and pumping equipment are required at facility to pressurize the CO_2 to a dense phase fluid. These were sized for each facility, considering the maximum emissions, using the equations from Ogden (2004).

The fixed operating costs consisted of maintenance in all cases. For the sources that required capture retrofitting, additional costs were incurred. These included labor, chemicals, catalysts and a cost associated with the energy penalty of capturing, rather than recycling, the CO_2. The variable costs were dependent on how much CO_2 was captured at each facility, which affects the energy costs for both compression and pumping.

4.3.2 Transport Costs

The transportation costs were split into those associated with pipeline transport and those associated with shipping. The output network from the GIS model provides the lengths to calculate pipeline costs. The equation from Essandoh-Yeddu and Gülen (2009) for the modified MIT model was used to calculate the cost per inch-mile, using data from

Oil and Gas Journal (2009 and 2017). The data detailed the cost breakdown for labor, ROW, materials and miscellaneous expenses for 2007 and 2016. From these, the relevant escalation factors were obtained. For offshore pipeline arcs an additional cost multiplier of 2 was used (Serpa et al., 2011). Three pipeline sizes were selected: 4, 8 and 12-inch diameter. These were selected in line with the possible range of CCS demands for the region.

Variable costs consider the pumping energy requirements to ensure the CO_2 is delivered to the wellhead in the dense phase by assuming a pressure drop per unit length of 49 Pa/m. Although these costs would be realized at the capture location, they were assigned to the transportation network due to the dependence on distance traveled. This ensures that the CO_2 is delivered to the storage location at the injection pressure. However, the model did not consider the placement and operation of booster stations as it was noted, on average, they are placed 200 km apart, which is greater than the distance between candidate sources and reservoirs (McCollum and Ogden, 2006).

For ship transport, the capacity in the case study was selected to be 10,000m^3. It was assumed the journey would take 2 days for distances under 200 km (IEAGHG, 2004; Ozaki et al., 2013). In addition, appropriate liquefaction and loading facilities were included in the costs for shipping. The power and water requirements for liquefaction contributed to the variable shipping costs. It was assumed that the ships have the required heating and pumping capability to deliver the CO_2 to the reservoir at the required injection pressure.

4.3.3 Storage Costs

The storage costs were also split into two separate groups: site costs and well costs. Due to the extensive characterization of the Texas Gulf Coast, the pre-final investment

decision costs were reduced compared to a less explored region. These included appraisal costs arising from seismic acquisition, exploration wells and injection tests. The results from Table 9 were used to calculate fixed operating costs from recurring seismic and MMV activities, as these were given on a per unit area basis (NETL, 2014). Finally, liability costs were included. However, Texas House Bill 1796 doesn't specify the size of the liability fund for offshore storage. Therefore, for liability payments, the fixed cost per tonne of CO_2 injected was taken from ZEP (2011c).

In addition to the site costs, well costs were calculated. These were field dependent and considered the depth to the top of the Lower Miocene formation at each site. The analysis utilized existing wells, as this was shown to be between 50-60% cheaper than drilling new wells (ZEP, 2011c; King et al. 2014). The associated equipment costs, including distribution lines, headers and electrical services were also included (McCollum and Ogden, 2006).

For all of the cost calculations, the dollar value from the corresponding literature was converted to 2017 dollars, using the CPI. It was also assumed that fixed and variable costs remained constant for the duration of a time period. These costs were then discounted back to year 0 values.

4.4 SCENARIOS

Several different demand scenarios were considered. The base case scenario considered two 12-year periods, with the total period 1 demand being 25 $MtCO_2$. These values were chosen as they represent current feasible CCS demands for early stage demonstration projects in the region. The Department of Energy's CarbonSAFE initiative seeks to develop a commercial scale project capable of storing 50 $MtCO_2$. Splitting this over two time periods results in the 25 $MtCO_2$ base case demand for period 1. Additionally,

a 12-year period was chosen as this is the duration over which businesses can take advantage of the Section 45Q tax credits for CCS. Beyond this 12-year period, the incentives and so demand for CCS projects are unknown. The complete list of scenarios is shown in Table 11.

Table 11. The demands and probability distributions of the different scenarios. The demands in period 2 are in addition to the mass stored during the first period.

Scenario	Demand, $MtCO_2$				Probability			Comments
	Time 1	Time 2						
		Low	Medium	High	Low	Medium	High	
1	25	50	60	70	0.3	0.4	0.3	
2	25	30	60	90	0.3	0.4	0.3	
3	25	30	40	50	0.3	0.4	0.3	
4	25	0	5	10	0.3	0.4	0.3	
5	25	0	30	60	0.3	0.4	0.3	
6	25	0	30	60	0.2	0.2	0.6	
7	25	0	50	100	0.3	0.4	0.3	
8	25	0	50	100	0.2	0.2	0.6	
9	25	0	5	10	0.3	0.4	0.3	6-year periods
10	25	0	50	100	0.3	0.4	0.3	Period 2 penalty

Chapter 5: Results

These 10 different scenarios were implemented in the optimization model, considering the candidate network, from GIS, linking all 12 sources to the 5 selected reservoirs. The stochastic solution was assessed using metrics such as the expected value of perfect information (EVPI) and value of stochastic solution (VSS). The results showed a large variation in VSS, suggesting that the difference from the expected value solution is not only dependent on the range of possible future values, but also on network characteristics that are specific to the capacities of the available sources and sinks.

The results are presented in three parts. Firstly, the generation of the candidate network from GIS is shown. Then, the output of the case two optimization is presented to demonstrate the differences between the perfect information, expected value and stochastic solutions. The variation in the results are highlighted and explained. In the third part, important findings are presented by highlighting specific differences between scenarios and their corresponding results.

5.1 GIS Output

The GIS model was run, considering the 12 sources and 5 selected reservoirs. A candidate network was generated consisting of 55 nodes and 132 arcs (72 pipelines and 50 ship routes), Figure 12.

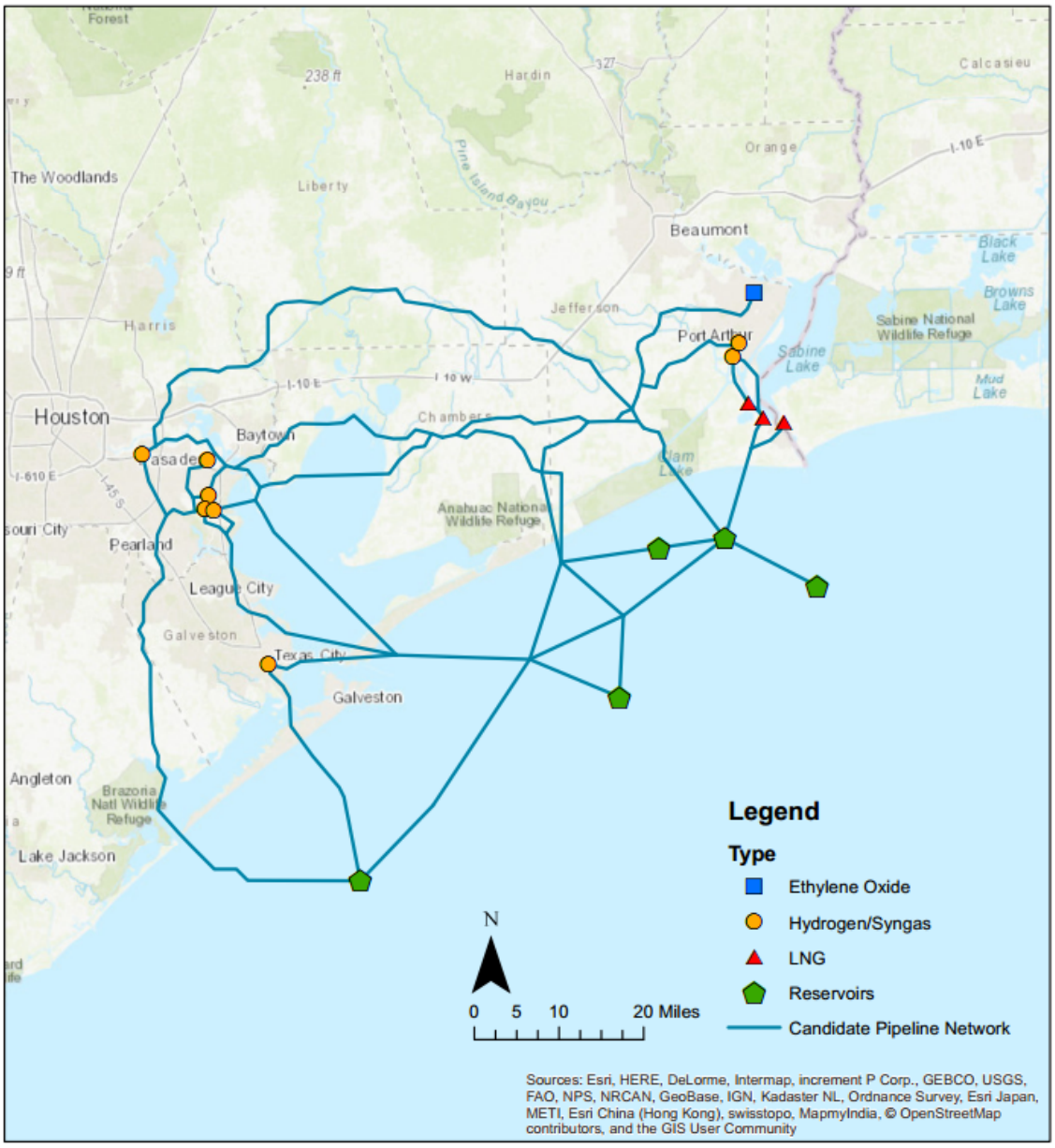

Figure 12. The generated candidate pipeline network, connecting the sources to reservoirs

5.2 Scenario 2 Output

The candidate network was input into the optimization model with cost data for the different sources, sinks and transportation modes. Optimal integrated networks were

generated for the scenarios in Table 11. Results from scenario 2 are used to demonstrate the output of the optimization model and show how the solutions differ between those which consider perfect information, the expected future value and future uncertainties. They indicate that, contrary to previous literature, a 'wait and see' approach provides the optimal stochastic solution, with larger, more costly infrastructure built in period two to take advantage of the time value of money. Additionally, the optimal solution is obtained by reducing the total amount of infrastructure built and so increasing the utilization across both time periods.

The model was run for scenario 2 utilizing the candidate network in Figure 12. This case considers the demands in Table 12. The symmetric probability distribution results in an expected future value of 60 $MtCO_2$.

Table 12. Scenario 2 demands and probability distribution

Demand, $MtCO_2$						
Time 1	**Time 2**			**Probability**		
	Low	**Medium**	**High**	**Low**	**Medium**	**High**
25	30	60	90	0.3	0.4	0.3

The optimal infrastructure was calculated for perfect information, the expected future value and uncertain future values. The visualization of the model outputs are presented in Figures 13 to 15 for each case. It should be noted the detour in the second stage network for the 90 $MtCO_2$ case, considering both the stochastic and perfect information solution, results from the flexibility in the model to allow CO_2 to flow in either direction along a pipe. This could be remedied by including least cost paths between all of the sources in the candidate network.

The first stage solutions represent action that would be taken now and the second stage solutions represent the subsequent action taken depending on the future realization of CCS demand, whether it be low, medium or high. The color and size of the circles in the figures indicates the amount of CO_2 captured or stored at each source and sink in a given time period. Additionally, the color of the arcs represents how much CO_2 flows along a given route.

Immediately, it is apparent that multiple solutions are common between the perfect information, expected value and stochastic cases. This results from the finite number of combinations of sources, sinks and transportation routes that can be selected. However, it also demonstrates the flexibility within the system as a whole: with a given infrastructure network the amount captured, transported and stored at each point can be varied within a range. For the low and high future demand cases, the perfect information solution is identical to the stochastic solution. Whereas for the medium future demand case, the perfect information and expected value solutions are the same. The results in Table 13 also demonstrates these similarities.

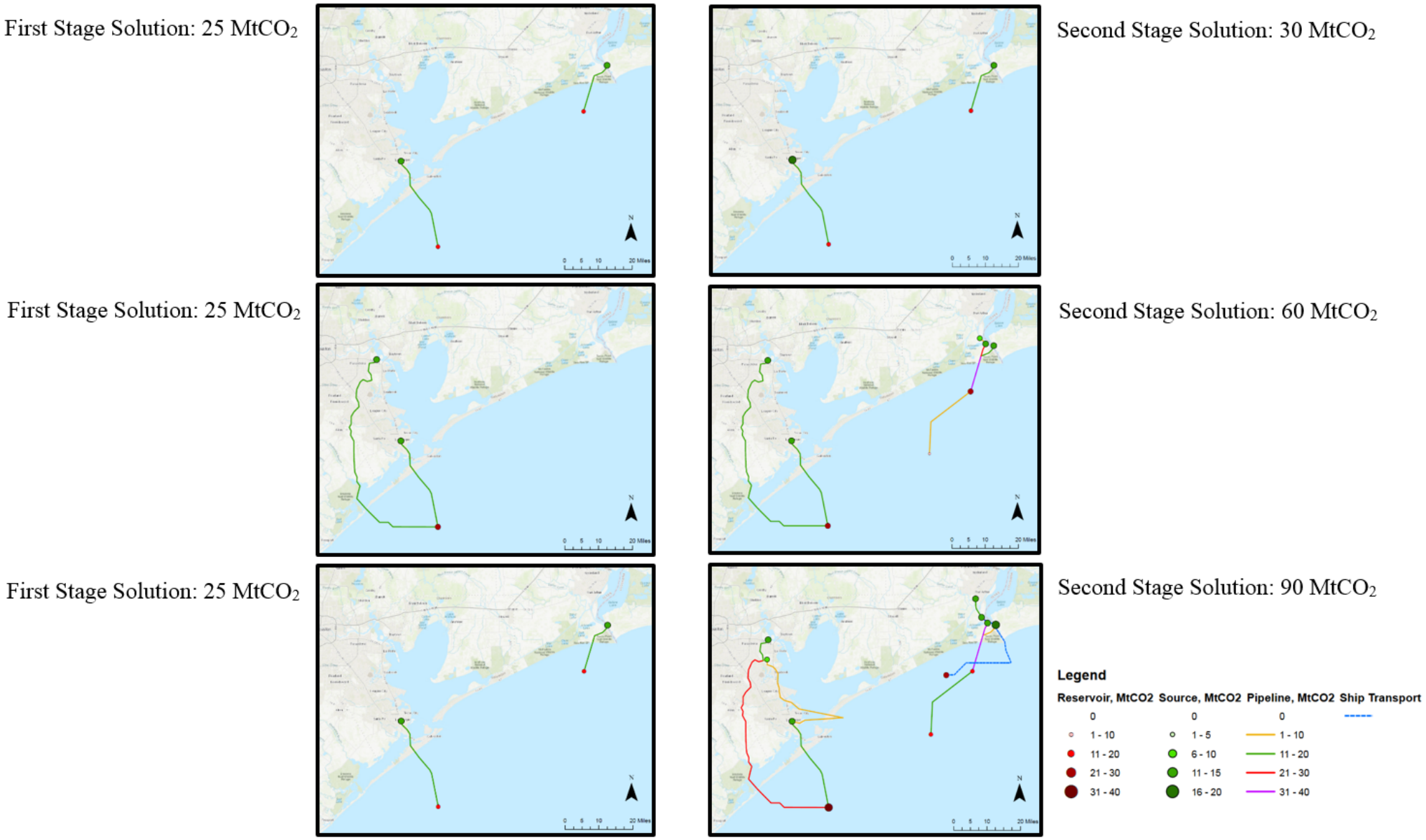

Figure 13. First and second stage networks for the perfect information solutions (Scenario 2 in Table 11)

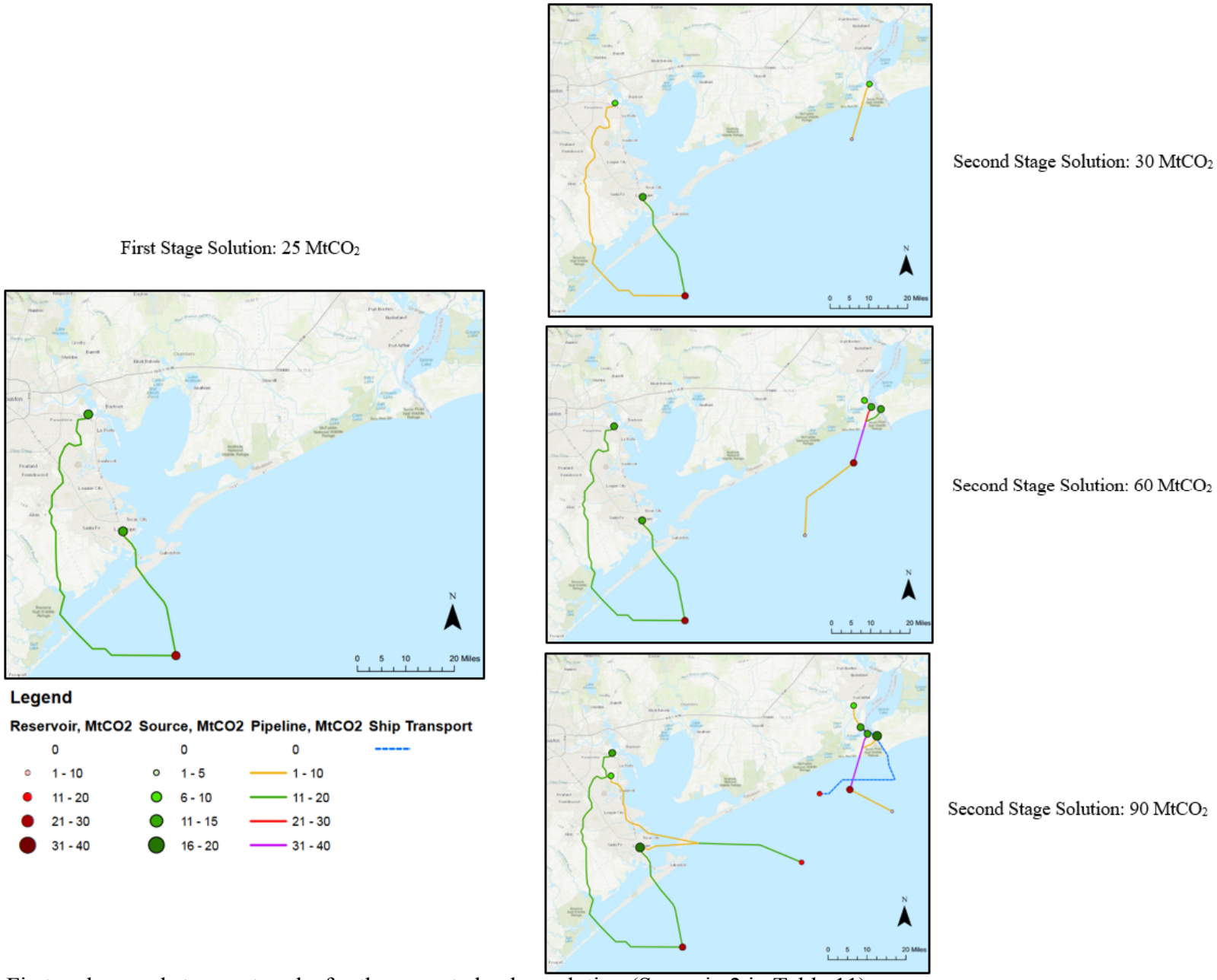

Figure 14. First and second stage networks for the expected value solution (Scenario 2 in Table 11)

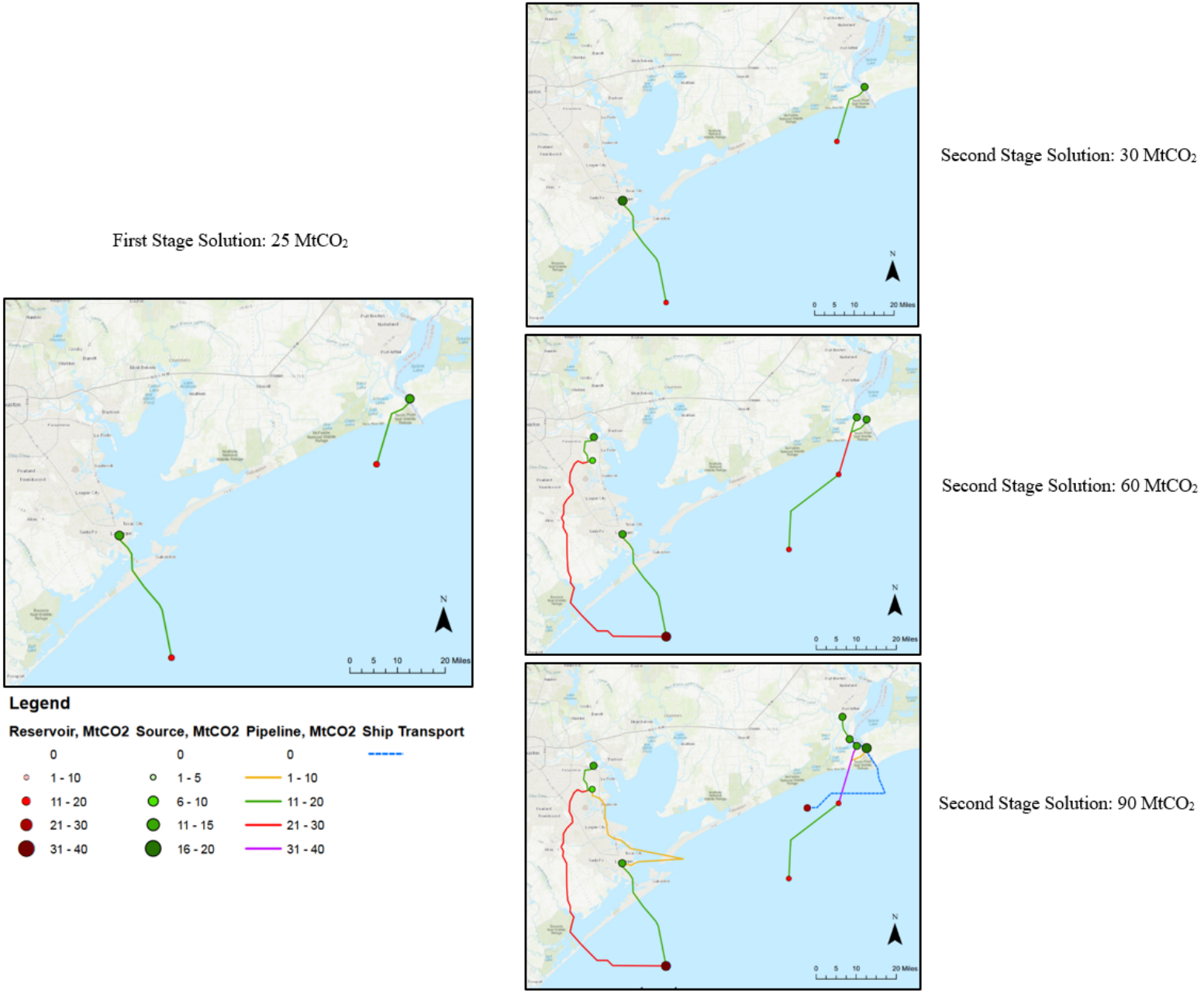

Figure 15. First and second stage networks for the stochastic solution (Scenario 2 in Table 11)

Table 13. Network costs in \$ x 10^6 for the perfect information, expected value and stochastic solutions

Scenario	Period 1 Low	Period 1 Medium	Period 1 High	Period 2 Low	Period 2 Medium	Period 2 High	Average Total
Perfect Information	438.7	485.7	438.7	140.4	328.0	723.2	847.7
Expected Value		485.7		151.9	328.0	691.2	869.8
Stochastic		438.7		140.4	377.4	723.2	848.7

Although the optimization considers capital costs, fixed operating costs and variable costs, in the majority of cases the optimal solution occurs when the infrastructure build out, and so capital expenditure, is reduced. This results from the fact that many fixed operating costs are expressed as a percentage of capital costs and that variable costs are dependent on the flow of CO_2, which is dictated the system demand. For case 2, capital costs make up 52-70% of the total system costs.

For the 30 and 90 $MtCO_2$ future demand cases, this reduction in infrastructure is achieved by utilizing the closest source-sink pairs. This is seen in both the perfect information and stochastic solutions. In these identical build outs, a pipeline network of 74km is built from two sources, each of which have pre-existing capture facilities, and as a result have low capital costs. These sources are located close to the coast, so reducing the distance to the available reservoirs.

However, the 60 $MtCO_2$ perfect information solution demonstrates that this shortest distance, least cost solution doesn't always provide the lowest costs over both time periods. In this case, reduction of infrastructure costs is achieved through not only selecting the cheapest sources, reservoirs and transportation options, but also by considering the utilization. By maximizing utilization, the total infrastructure requirements are reduced.

The results in Table 13 demonstrate the period 1 cost for the perfect information scenario to be $485.7 million compared to $438.7 million for the stochastic solution. However, the period 2 costs show the perfect information solution to be $49.4 million less expensive than the stochastic network.

These results can be explained by considering reservoir 3, in the south-west corner of the map. For the future demand of 60 $MtCO_2$ the perfect information solution selects a longer network in period 1, 169 km, compared to the stochastic solution, 74 km. This initial infrastructure investment allows reservoir three to be fully utilized by the end of period 2 without requiring any additional pipelines, with 25 $MtCO_2$ injected in period 1 and 26 $MtCO_2$ in period 2. Whereas in the stochastic solution, an additional 12" diameter pipeline has to be built in period 2 to increase the injection into this reservoir from 13 $MtCO_2$ to 34 $MtCO_2$ and so increase its utilization. The utilization for the perfect information, expected value and stochastic solutions for scenario 2 are shown in Table 14.

Table 14. Utilization of each of the three sub-systems for scenario 2 with a 60 $MtCO_2$ future demand.

		Capacity Utilization, %					
		Time 1			Time 2		
		Source	**Transport**	**Sink**	**Source**	**Transport**	**Sink**
Perfect Information	Low	71.6	94.9	36.7	86.1	79.4	88.5
	Medium	81.1	93.8	49.0	82.9	83.9	81.7
	High	71.6	94.9	36.7	98.3	74.0	92.4
Expected Value	Low	81.1	93.8	49.0	67.6	69.2	63.1
	Medium	81.1	93.8	49.0	82.9	83.9	81.7
	High	81.1	93.8	49.0	97.6	75.1	85.6
Stochastic	Low	71.6	94.9	36.7	86.1	79.4	88.5
	Medium	71.6	94.9	36.7	89.7	76.2	85.7
	High	71.6	94.9	36.7	98.3	74.0	92.4

It should be noted, for reservoirs the capacity is a volume, or mass, of carbon dioxide. Whereas for sources and transportation it is a mass flow rate. Therefore, as expected the utilization of reservoirs always increases over time as the capacity is filled.

The utilizations in Table 14 elucidate some important results. The high capital costs of building infrastructure mean that sources, pipes, ships and reservoirs are used near their capacity before additional infrastructure is brought online. Additionally, it can be seen that the utilization of transportation drops in period 2 compared to period 1. This is in contrast to prior literature, which suggest overbuilding transportation routes provides the optimal pathway for developing integrated networks in the future. Instead the results demonstrate a ‘wait and see approach’. In this approach low cost networks built in period 1 aim to

maximize infrastructure utilization. In period 2, additional infrastructure is added to adapt to the realized demand. This additional infrastructure benefits from time value of money with larger pipelines being built in these later periods. The discount, therefore reduces the benefit of overbuilding capacity in period 1 and instead incentivizes waiting. The transportation build out in the medium demand scenario provides a good example of this, with no 12" diameter pipeline built in period 1, yet 24 km and 122 km of 12" pipeline built in period 2 for the perfect information and stochastic solutions, respectively.

Finally, it is observed that the selection of sources and reservoirs in the corresponding solutions for perfect information, expected value and future uncertainty remain relatively constant. The maximum flexibility arises from the selection of transportation routes and modes. This presents options for whether to use pipeline or ship transport, the diameter of the pipeline and the route to follow. These costs are on the same order as capture costs. For the perfect solution with a future demand of 60 $MtCO_2$, the total costs associated with sources, sinks and transportation are $363 million, $145 million and $306 million respectively. It is therefore expected that the maximum benefit of a stochastic solution over the expected value solution is predominantly achieved via near term hedging of the transportation infrastructure.

Additional cases are presented to demonstrate how this value of stochastic solution varies with uncertainty and demands, as well as how the expected value of information changes. Figure 16 demonstrates the value of stochastic solution for case two.

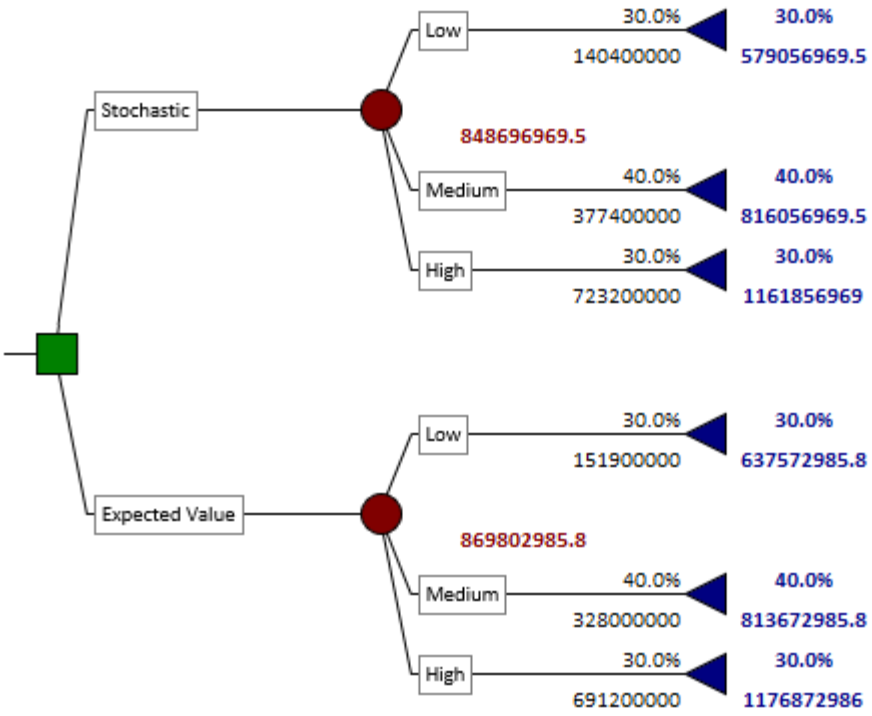

Figure 16. Decision tree showing the expected cost of the stochastic and expected value solutions in red. The second stage costs associated with each recourse action are shown in black.

5.3 Additional Results

The optimization outputs from the 10 different scenarios were used to calculate the expected total cost of the stochastic solution. Additionally, deterministic results were calculated by considering i) perfect information about the future state of the world and ii) expected future value to generate a first stage solution and recourse decisions. The VSS (difference expected value solution and stochastic solution) and EVPI (difference between perfect information solution and stochastic solution) were presented. These results can be seen in Table 15. Detailed results are listed in Appendix D.

Table 15. Total system costs for perfect information, expected value and stochastic solutions. The VSS and EVPI are shown as both absolute and relative values.

Scenario	Demand, $MtCO_2$ (% Probability) Time 1	Time 2 Low	Time 2 Medium	Time 2 High	System Cost, $ x 10^6 Perfect Information	Expected Value	Stochastic	EVPI (%)	VSS (%)
1	25	50 (0.3)	60 (0.4)	70 (0.3)	812.6	813.7	813.7	1.1 (0.1)	0.0 (0.0)
2	25	30 (0.3)	60 (0.4)	90 (0.3)	847.7	869.8	848.7	0.9 (0.1)	21.1 (2.5)
3	25	30 (0.3)	40 (0.4)	50 (0.3)	654.6	660.5	657.8	3.1 (0.5)	2.8 (0.4)
4	25	0 (0.3)	5 (0.4)	10 (0.3)	465.4	465.4	465.4	0.0 (0.0)	0.0 (0.0)
5	25	0 (0.3)	30 (0.4)	60 (0.3)	610.6	611.3	611.3	0.7 (0.1)	0.0 (0.0)
6	25	0 (0.2)	30 (0.2)	60 (0.6)	693.9	701.3	695.3	1.4 (0.2)	6.0 (0.9)
7	25	0 (0.3)	50 (0.4)	100 (0.3)	813.6	833.9	818.0	4.4 (0.5)	15.9 (1.9)
8	25	0 (0.2)	50 (0.2)	100 (0.6)	1012.2	1032.3	1014.7	2.5 (0.2)	17.6 (1.7)
9	25	0 (0.3)	5 (0.4)	10 (0.3)	653.1	654.4	654.4	1.3 (0.2)	0.0 (0.0)
10	25	0 (0.3)	50 (0.4)	100 (0.3)	1459.6	1534.8	1527.7	68.0 (4.5)	7.2 (0.5)

The low EVPI values seen for the majority of cases demonstrate the inherent flexibility in the integrated network. This means that the infrastructure selection in period 1, for the stochastic solution, allows it to adapt once the future state of the world is realized. This also shows that there is little value in making the future demand more certain. The results also show that there is no intuitive or obvious set of scenarios in which the stochastic solution performs better than the expected value solution.

The results from scenarios 2, 6, 7 and 8 show the greatest values of the stochastic solution. Initially, it appears this occurs as a result of these scenarios having the greatest uncertainty ranges. This certainly contributes and can be deduced logically by considering the opposite: if the range of future values tends to zero then the problem merely becomes a deterministic problem and the value of stochastic solution will decrease to zero. However, by comparing scenarios 5 and 6 it can be seen the assertion that a large future value range will lead to a large value of stochastic solution doesn't always hold. These two scenarios share the same properties apart from their future value probabilities. Hence, their expected values are different. In case 5, there is no difference between the naïve approach (expected value solution) and the stochastic solution. However, in case 6 there is a 0.9% difference. This difference arises from larger pipeline diameters being selected in the latter case due to the higher expected future value. When the future states of the world are realized, this first stage selection forces a sub-optimal selection of subsequent routes.

The opposite can also be seen: that having a certain expected value will not always lead to a certain value of stochastic solution. Cases 1 and 2, have the same expected future values but different future demand distributions. Therefore, to determine whether a stochastic solution will have value, both the expected value and future possible states of the world must be considered. The importance of each is dependent on network characteristics such as source, reservoir and pipe capacities and costs.

The selection of sources is similar between the expected value solutions and the stochastic solutions. However, the pipeline routes vary considerably. Due to the similarity between source selection, the observed VSS is a small percentage of total costs, up to 2.5%. However, the next most costly aspect, transportation, shows that compared to the expected value solution the stochastic solution can have larger relative savings.

Table 16. The value of stochastic solution for the transportation network as a percentage of the stochastic transportation solution

Scenario	Value of stochastic solution for transportation subsystem, %
1	0.0
2	12.5
3	-2.4
4	0.0
5	0.0
6	9.6
7	14.0
8	7.6
9	0.0
10	2.2

The scenarios shown to have the greatest overall VSS also have the largest transportation cost savings. Savings up to 14% are created by implementing the stochastic solution rather than the expected value solution. In case 3, the transportation is seen to be marginally more expensive in the stochastic solution compared to the expected value solution. However, the total system cost is lower for the stochastic solution due to lower capture and storage costs.

The results show other important trends for CCS network development. Firstly, cases 4 and 9 show decreasing scenarios. These demonstrate that there is no value in including future uncertainty if it is known that CCS demand will be lower than it is today.

In every case, the recourse action will be to stop using the infrastructure. The flexibility offered by the stochastic solution will therefore have no impact on these scenarios. This is in contrast to scenarios 6, 7, and 8, in which a decrease represents only one of the possible three future demands. In these scenarios, there is a benefit over the expected value solution.

Additionally, the length of each period is important with these decreasing future demands. Scenario 9 utilized ship transport in period 1 and sold these in period 2 depending on which demand was seen, Table 24. This validates the assertions from prior literature that ship transport can be beneficial in uncertain situations. However, if the length of the period is doubled, scenario 4, then no similar action is observed. The residual value of the ships is reduced and so they are less likely to be considered in scenarios with a time period over a certain length. Therefore, uncertainty is not the only prerequisite for ship transport, but the length of the project and ship life has to be considered too. These additional values are important because they determine the offered by the ship at the end of period 1. These shorter time periods give a better representation of reality, in which decisions can be made at any point and policies are likely to concentrate on the near term.

The time value of money in period two allows value to be gained from waiting before committing to action, as a result of the discounted costs. Comparing scenarios 7 and 10 demonstrates the benefits associated with the discount factor. In scenario 10, a penalty was used to dissuade delay of action. This penalty could result from certain externalities, such as competition for resources against a growing LNG industry. This factor affects all costs in period 2 and yields different results from changing demands or uncertainties. It highlights the importance of considering what the costs of future CCS deployment are likely to be. By including a penalty multiplier on period 2, and thus increasing the associated costs, the VSS decreases by 1.4% but the EVPI increases by 4%. It also reduces the ability for a stochastic solution to provide flexibility for future states of the world and

instead incentivizes developing now. As a result, the most benefit in this scenario is through understanding the future need for CCS and acting accordingly. Up to $68 million would be paid to know the future need for CCS before building any infrastructure, which represents 4% of the total costs. However, in practice reducing the uncertainty of CCS is difficult due to the number of external factors that influence it. Determination of the discount, or penalty, in future models will be key, as it can significantly impact the outcome of the optimization and planning decisions made.

Chapter 6: Conclusion

There exists a wide range of uncertainties in the development and deployment of CCS. These uncertainties should be considered when developing and planning a CCS network. However, models to date have either neglected these, or not considered the spatial aspects of network planning. The model presented in this paper is the first to consider both uncertainty and spatial distribution of sources and reservoirs in CCS network optimization. GIS and mixed integer programming were combined to yield a result that was optimal, and easily interpreted via map visualizations.

A case study on the Texas Gulf Coast looked at building a network between 12 emissions sources and 5 reservoirs, for 10 different demand scenarios. Three main conclusions can be drawn from the results. Firstly, the importance of developing the stochastic solution is dependent on many factors including the future demand distribution. Secondly, the time period considered can alter the pathway taken even when all other variables are held constant. Finally, the second stage discount factor can change the strategy from a delayed to an early action approach

Cost reductions were observed when a stochastic optimization was run and compared to a 'naïve' approach in which only the expected value of future demand was considered. These solutions reduced total system costs by maximizing infrastructure utilization. However, the situations in which a stochastic solution provides appreciable savings are neither obvious or intuitive. They depend on multiple factors including expected value and uncertainty range of future demands. In particular, it is important to understand how the expected value relates to the capacities in the candidate network. As a result, there is benefit in considering the stochastic solution as it can elucidate some non-

obvious least cost pathways. At worst, the stochastic solution will equal the expected value solution.

In considering early stage networks, it was also observed that the majority of cost savings were achieved through optimal selection of pipeline sizes and routes. The selection of sources, which contribute to the greatest proportion of overall costs, were seen to remain steady across the scenarios. This resulted from the relatively, constant capital costs observed for high purity sources. However, the variation in transportation options led to savings of up to 14% when uncertainty was included in the model. Transportation modes were also seen to be heavily dependent on the period length for the given simulation. When this value was decreased from 12 to 6 years more ships were utilized as they provide residual value via resale.

Finally, applying a penalty rather than a discount to period two takes the option value away by effectively incentivizing early action. This can have large effects on the optimal stochastic strategy, with the value of the stochastic solution decreasing and the expected value of perfect information increasing. This suggests that as the penalty is increased the expected value of perfect information will also increase. This penalty could be important in future scenarios where it is likely there will be increased competition for resources and labor from similar industries.

Chapter 7: Future Work

Multiple areas of possible refinement exist within each of the models. For the network generation in GIS, additional complexity can be added to further reduce costs and to enable greater flexibility in the optimization model. These modifications could include the consideration of utilizing existing rights of way or reusing pipelines. The shipping routes should also be modified to allow multi-stop trips: collecting CO_2 from multiple docks before heading to the well site. The GIS model should also be modified to ensure each source is not only connected to all the reservoirs, but to all of the other sources too.

Due to the nature of the CPLEX optimization, it is difficult to add extra functionality without significantly lengthening the solve time. Therefore, future development should initially concentrate on implementing more efficient ways to solve the optimization problem. Further investigation into the importance of the discount factor should be used to approximate the point at which the equilibrium between pipeline and ship costs is reach. Additionally, the model could easily be adapted to consider other uncertainties. One particularly interesting application would be to consider emissions uncertainty while trying to reach a target CCS demand. This would have to consider the tradeoff between certainty of emissions, the cost for capture and possible construction durations.

Future development isn't restricted to CCS networks. Multiple other applications could make use of the framework and methodology. This includes wastewater disposal from shale development. This waste stream can't be disposed of directly into waterways, well site conditioning is expensive and some states don't have the suitable geology for subsurface disposal. Therefore, the model could be used to determine the optimal solution between well site treatment and transferring for disposal in a neighboring state.

APPENDICES

Appendix A

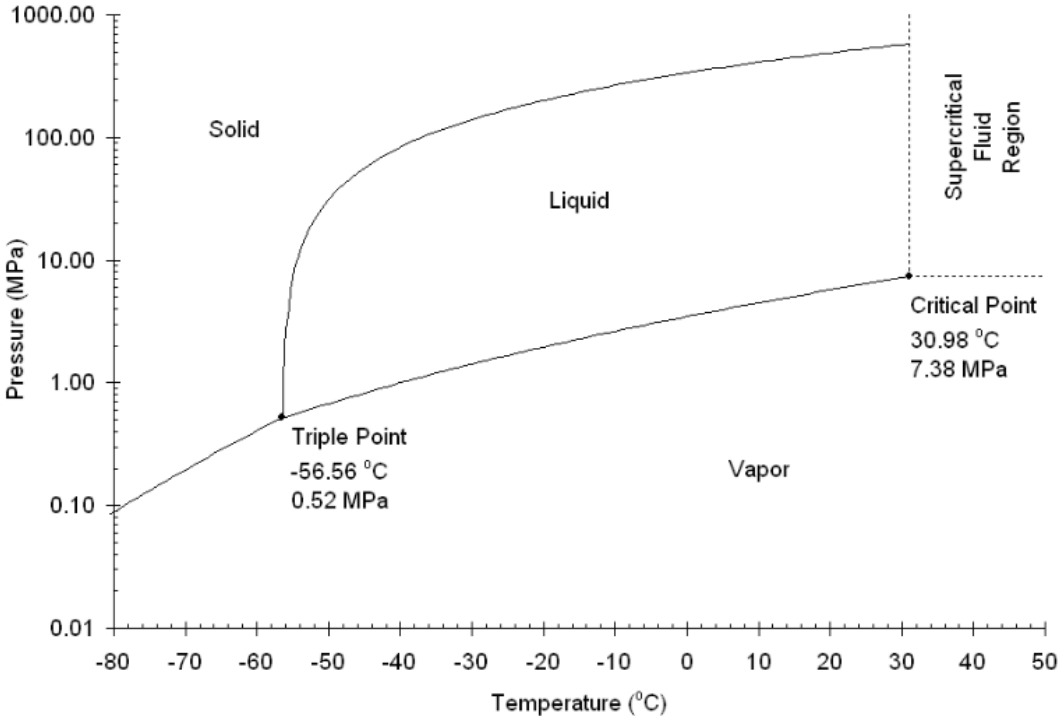

Figure 17. A phase transition diagram for CO_2 with the critical point marked. Dense phase refers to CO_2 in the liquid or supercritical region (McCoy, 2007).

Appendix B

The costs for the two-stage solution were calculated considering the time value of money. Capital investment was made in the first year of each time period, whereas O&M costs and variable costs were annual payments for the duration of the period. The O&M and variable costs were assumed to be constant throughout the time period. Therefore the value discounted to the initial year of any given period was determined by multiplying by the following factor:

$$DV_f = \sum_{n=1}^{N} \frac{1}{(1+r)^{(n-1)}} \qquad (B1)$$

Where n is the year number, N is the total number of years in a period and r is the discount rate. For the study, a discount rate of 8% was used. This is in line with values used in other studies (ZEP, 2011a; 2011b; Roussanaly et al., 2013; Fimbres Weihs et al., 2014; IEAGHG, 2017).

Once the discounted value to the start of a given period was determined, the present value was deduced by multiplying by:

$$PV_f = \frac{1}{(1+r)^{(n-1)}} \qquad (B2)$$

All prices were adjusted to 2018 dollars where applicable using the CPI. For all calculations, the commercial electricity rate for Texas, from January 2018, was used (EIA, 2018)

Capture

All of the selected sources have CO_2 capture or separation currently employed. However, 5 out of the 12 only utilize PSA. These sources are all facilities that produce hydrogen via steam methane reforming. Therefore, the cost estimates from IEAGHG (2017) were to determine the cost of additional capture on the exit stream of the PSA. This

provides the most probable route for retrofitting existing plants. These costs were scaled in line with the output of each facility compared to the one in the study. For sources with existing capture facilities, only compression and pumping requirements were added.

Table 17. Capture cost calculations

Cost	Source
Capital Cost:	
Capture plant: $69,500,000	For a 100,000 MMSCF per day hydrogen plant IEAGHG(2017)
Compressor Costs: $\dot{m}\left[0.13 \cdot 10^6 \dot{m}^{-0.71} + 6.02 \cdot 10^6 \dot{m}^{-0.6}\right]$	McCollum and Ogden (2006), $\dot{m}$ in kg/s
Pump Costs: $\left[1.11 \cdot 10^6 \frac{0.187\dot{m}}{1000}\right] + 0.07 \cdot 10^6$	McCollum and Ogden (2006), $\dot{m}$ in tonnes/day
Fixed O&M:	
Capture Plant: 1.5% of Capital Cost annually multiplied by DVf	For a 100,000 MMSCF per day hydrogen plant IEAGHG(2017)
Compressor and Pump: 4% of Capital Costs annually multiplied by DVf	McCollum and Ogden (2006) IEAGHG(2017)
Labor, Chemicals and Catalysts: $813,600 annually multiplied by DVf	For a 100,000 MMSCF per day hydrogen plant IEAGHG(2017)
Fuel Penalty: $3,315,000 annually multiplied by DVf	
Variable Cost: $\$4,665,000 \cdot DV_f \frac{T}{n}$	Modified from McCollum and Ogden (2006)

Pipeline Costs

Pipeline costs comprised of the capital costs, fixed O&M and variable pumping costs. Although pumping would be performed at the capture facility, the pressure drop, and so pump work required, is dependent on arc length. These calculations were implemented after the network construction in the GIS model. The table below gives the pipeline cost breakdown:

Table 18. Pipeline cost calculations

Cost	Source
Capital Cost: $\frac{(\eta\gamma\alpha\beta)}{(\gamma+\alpha+\beta)} * \$62{,}967\ inch/km$ $\eta = 1.455$ $\gamma = 1.271$ $\alpha = 2.882$ $\beta = 1.588$ $\Rightarrow \$92{,}817\ /inch/\text{km}$	Essandoh-Yeddu and Gülen (2009) Escalation factors, $\eta, \gamma, \alpha, \beta$, were determined from Smith (2009) and Smith (2017)
Offshore cost multiplier: 2	Serpa et al. (2011)
Fixed O&M: 4% of Capital Costs annually multiplied by DVf	McCollum and Ogden (2006) and NETL(2013)
Variable Cost: $DV_f \frac{TL}{n} \frac{10{,}000\Delta P}{36\rho\eta_p} p_e CF$ $\Rightarrow \$1.889\ \frac{TL}{n} \cdot\ DV_f$	Modified from McCollum and Ogden (2006) T: Total CO_2 demand for period, $MtCO_2$ N: Number of year in period L: Length of arc, m ΔP: Pressure drop per unit length, Pa/m ρ: CO_2 density in kg/m^3 η_p: pump efficiency p_e: Commercial electric rate in \$/kWh CF: pump capacity factor

Shipping Costs

The shipping costs assumed the CO_2 was delivered under pressure. This simplifies the cost calculations for the compression and pumping because the delivery pressure is the same no matter whether it is to the ship terminal or wellhead. It was also shown to produce cheaper costs overall (IEAGHG, 2004). A round trip, including loading and unloading, was taken to be 2 days (IEAGHG, 2004 and GCCSI, 2011), resulting in 2.1 $MtCO_2$ $ship^{-1}$ $year^{-1}$. Certain variables, such as fuel costs and roundtrip time were assumed to be constant for all routes as these were found to be weakly dependent on distance if the journey is less than 1000km. A conversion rate of 0.638 EUR to USD was used for the ZEP (2011b) conversion.

Table 19. Shipping cost calculations

Cost	Source
Capital Cost:	
Ship: $45,500,000	IEAGHG (2004) for 10,000m^3
Buffer Storage: $17,200,000	ZEP (2011b) for floating barge storage
Liquefaction: $20,100,000	IEAGHG (2004) scaled to 10,000m^3day^{-1}
Loading Arms: $10,700,000	IEAGHG (2004)
$\Rightarrow \$93{,}500{,}000/ship$	
In addition the pipeline costs from the source to dock was added to the capital cost, for the given length. This was for a diameter with a capacity large enough to meet the maximum shipping capacity.	
Fixed O&M:	
Ship (including labor): 5% of capital costs annually	IEAGHG (2004)
Loading Arm: 2% of capital costs annually	ZEP (2011b)
Buffer Storage: 5% of capital costs annually	ZEP (2011b)
Fuel: $2,350,000 annually	IEAGHG (2004)
Liquefaction Labor: $300,000 annually	ZEP (2011b)
$\Rightarrow \$6{,}000{,}000 \cdot DV_f\ /ship$	
Variable Cost:	
Harbor Fee: $5,050,000 $MtCO_2^{-1}$	IEAGHG (2004)
Liquefaction Water: $8,100,000 $MtCO_2^{-1}$	ZEP (2011b)
Liquefaction Power: $1,100,000 $MtCO_2^{-1}$	IEAGHG (2004)
$\Rightarrow \$7{,}000{,}000 \cdot DV_f\ \frac{T}{n}$	

Storage

The storage costs were split up into two sections: site preparation and injection wells costs. As the area is well characterized due to the oil and gas activity, no exploration wells are needed (ZEP, 2011c). Additionally, due to the extensive seismic data in the

region, no pre-injection characterization costs are incurred. The costs associated with the liability fund and 4D seismic acquisition are spread across the operating period. It was also assumed that the existing platforms has sufficient life left to cover the length of the project.

Table 20. Storage cost calculations

Cost	Source
Capital Cost:	
Injection Test: $1,450,000/site	ZEP (2011c)
Storage Permit: $1,450,000/site	ZEP (2011c)
MMV:	
Drilling cost: $w \cdot 10^6 \cdot 0.1381e^{0.0008d}$	McCollum and Ogden (2006) w: Number of wells; d: depth of well, m
Re-use (work over): 0.6 drilling cost	ZEP (2011c)
Number of wells (w) : 0.75 wells/mile^2	NETL (2014)
Contingency: 20% of capital costs	ZEP (2011c)
Post-injection monitoring: 10% of MMV annually, discounted back (10 years for Texas and Louisiana)	ZEP (2011c) Louisiana House Bill 661
Decommissioning: 15% of capital costs discounted back from the end of project	ZEP (2011c)
Fixed O&M:	
Seismic: $126,000 mile^{-2} every 5 years multiplied by DV_f	ZEP (2011c)
O&M: 4% capital costs multiplied by DV_f	ZEP (2011c)
Variable Cost:	
Liability: $1,700,000 $MtCO_2^{-1}$ $\Rightarrow \$1{,}700{,}000 \cdot DV_f \frac{T}{n}$	ZEP (2011c)

Wells

Well cost consist of the drilling and equipment cost. It is assumed that the CO_2 is delivered under pressure, so no additional pumping is required.

Table 21. Well cost calculations

Cost	Source
Capital Cost:	
Drilling cost: $w \cdot 10^6 \cdot 0.1381e^{0.0008d}$	McCollum and Ogden (2006) w: number of wells; d: depth in m
Re-use (work over): 0.6 drilling cost	ZEP (2011c)
Equipment: $w \cdot 49433\left(\frac{m}{280w}\right)^{0.5}$	McCollum and Ogden (2006) w: number of wells; m: maximum injection rate tpd
Contingency: 20% of capital costs	ZEP (2011c)
Decommissioning: 15% of capital costs, discounted back from the end of project	ZEP (2011c)
Fixed O&M:	
O&M: 4% capital costs multiplied by DV_f	ZEP (2011c)

Appendix C

Models were created to allow the calculation of density, viscosity and maximum mass flow rate for specific temperature and pressure operating conditions. The density of CO_2 was calculated using the Peng-Robinson equation, where both temperature and pressure were varied:

$$a = 0.45724 \frac{R^2 T_c^2}{p_c} \quad \text{(C1)}$$

$$b = 0.07780 \frac{RT_c}{p_c} \quad \text{(C2)}$$

$$\alpha = (1 + \kappa(1 - T_r^{0.5}))^2 \quad \text{(C3)}$$

$$\kappa = 0.37464 + 1.542266\omega - 0.26992\omega^2 \quad \text{(C4)}$$

$$T_r = \frac{T}{T_c} \quad \text{(C5)}$$

$$A = \frac{\alpha a p}{R^2 T^2} \quad \text{(C6)}$$

$$B = \frac{bp}{RT} \quad \text{(C7)}$$

$$Z^3 - (1 - B)Z^2 + (A - 2B - 3B^2)Z - (AB - B^2 - B^3) = 0 \quad \text{(C8)}$$

where R is the universal gas constant, Tc is the temperature at the critical point, pc is the pressure at the critical point, ω is the acentric factor and Z is the compressibility factor. The real roots of the equation were used to determine Z. Subsequently, the density was determined utilizing the equality:

$$\rho = \frac{Mp}{ZRT} \tag{C9}$$

where M is the molar mass in kg/mol and ρ is the density in kg/m^3. The model allows an average density factor to be determined depending on the expected average temperature and pressures. It was assumed the average temperature was constant and equal to the ground temperature of the pipeline route (McCoy and Rubin 2007 and Essandoh-Yeddu and Gülen, 2009).

The dynamic viscosity of the CO_2 was determined using the correlation presented by Bahadori and Vuthaluru (2010) that utilized 16 coefficients to give μ, in cP, in terms of T and p for temperatures between 260 and 340K and pressures between 10 and 70 MPa.

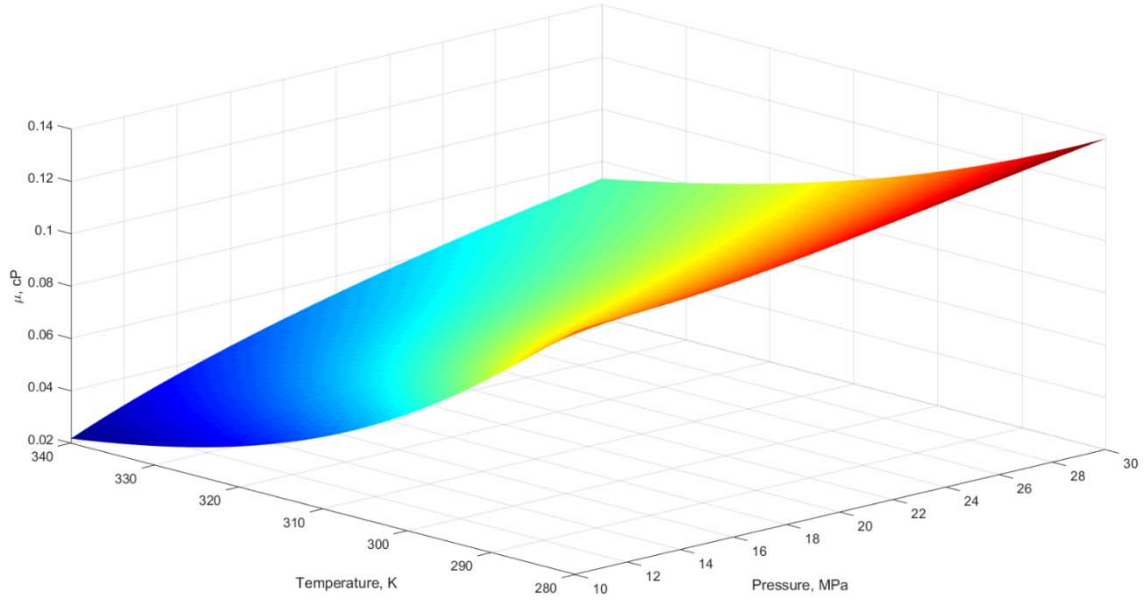

Figure 18. The viscosity of CO_2 as a function of pressure and temperature, calculated from Bahadori and Vuthaluru (2010)

Nominal pipe sizes (NPS) from 4 to 36-inch diameters were used for the calculations. The US Code of Federal Regulations (49 CFR § 195.106, 2005) defines the pipe thickness for a given outside diameter:

$$t = \frac{D_o p_{dp}}{2SEF} \tag{C10}$$

The thickness t is in meters, D_o is the outside diameter of the pipe in meters, p_{dp} is the design pressure, in Pa, S represents the yield strength of the material, E is the longitudinal joint factor, taken as 1, and F is the design factor, defined as 0.72 for this scenario. Once the thickness has been calculated, the inside pipe diameter can be determined for the nominal pipe size. It should be noted that NPS corresponds to the outside diameter for pipe sizes above 12 inches and the inside diameter for sizes less than or equal to 12 inches. Therefore, for the smaller pipe sizes wall thickness does not need to be calculated.

Many equations are presented that link mass flow rate, pipeline diameter and pressure drop per unit length. The equations fall into two broad categories: those based on the optimal economic design and the others that use energy-balance equations for turbulent flow in pipes. The equation proposed by Vandeginste and Piessens (2008) provided a simple form that was also dependent on elevation change. It was rearranged to the following form:

$$\dot{m} = \sqrt{\frac{D^5 \rho \pi^2 [\rho g (z_1 - z_2) + (p_1 - p_2)]}{8 f_D L}} \tag{C11}$$

with z_1 and z_2, and p_1 and p_2 being the elevation, in m, and pressure, in Pa, respectively of the pipe at points 1 and 2. The constant, g, is the gravitational acceleration in $kgms^{-2}$, D is the pipe inside diameter in m, L is the length of pipe segment in m and f_D is the Darcy-Weisbach friction factor.

The Darcy-Weisbach friction factor is given as a function of Reynold's number and relative roughness (Zigrang and Sylvester, 1982). The equation provides the most accurate approximation of the implicit Colebrook equation for calculating the friction factor (Genić et al., 2011).

$$f_D = \left\{-2log_{10}\left[\frac{\varepsilon}{3.7} - \frac{5.02}{Re}log_{10}\left(\varepsilon - \frac{5.02}{Re}log_{10}\left(\frac{\varepsilon}{3.7} + \frac{13}{Re}\right)\right)\right]\right\}^{-2} \quad \text{(C12)}$$

The equation includes ε, the relative roughness, which is taken to be $0.0457 \times 10^{-3}/D$. The Reynolds number is:

$$Re = \frac{4\dot{m}}{\mu\pi D} \quad \text{(C13)}$$

The prior equations have to be solved iteratively to obtain a maximum mass flow rate for each diameter. Although there was assumed to be no elevation change in the current optimization, the GIS model was coded to allow this to be considered in future.

Appendix D

Table 22. Detailed cost breakdown for each scenario under perfect information, displayed in $ millions

Scenario	Perfect Information Deterministic						
	Low		Medium		High		Average
	Time 1	Time 2	Time 1	Time 2	Time 1	Time 2	Total
1	485.7	239.6	485.7	328.0	469.5	428.9	812.6
2	438.7	140.4	485.7	328.0	438.7	723.2	847.7
3	438.7	140.4	438.6	219.7	485.7	239.6	654.6
4	438.6	11.0	438.6	28.2	438.6	40.8	465.4
5	438.6	11.0	438.7	140.4	485.7	328.0	610.6
6	438.6	11.0	438.7	140.4	485.7	328.0	693.9
7	438.6	11.0	485.7	239.6	484.3	811.2	813.6
8	438.6	11.0	485.7	239.6	484.3	811.2	1012.2
9	704.5	-81.7	704.5	-56.6	667.6	22.7	653.1
10	438.6	32.9	530.5	661.1	727.4	2077.8	1459.6

Table 23. Detailed cost breakdown for each scenario under the expected value solution, displayed in $ millions.

Scenario	Time 1	Expected Value Deterministic Low Time 2	Medium Time 2	High Time 2	Average Total
1	485.7	239.6	328.0	416.5	813.7
2	485.7	151.9	328.0	691.2	869.8
3	438.6	147.7	219.7	299.0	660.5
4	438.6	11.0	28.2	40.8	465.4
5	438.7	11.0	140.4	377.4	611.3
6	469.5	11.0	112.6	345.2	701.3
7	485.7	8.8	239.6	832.5	833.9
8	469.5	11.0	277.6	841.8	1032.3
9	704.5	-81.7	-56.6	-10.1	654.4
10	530.5	26.5	661.1	2439.9	1534.8

Table 24. Detailed cost breakdown for each scenario under the stochastic solution, displayed in $ millions.

Scenario	Time 1	Stochastic			
		Low Time 2	Medium Time 2	High Time 2	Average Total
1	485.7	239.6	328.0	416.5	813.7
2	438.7	140.4	377.4	723.2	848.7
3	438.7	140.4	219.6	297.1	657.8
4	438.6	11.0	28.2	40.8	465.4
5	438.7	11.0	140.4	377.4	611.3
6	438.7	11.0	140.4	377.4	695.3
7	438.7	11.0	297.1	857.4	818.0
8	438.7	11.0	297.1	857.4	1014.7
9	704.5	-81.7	-56.6	-10.1	654.4
10	484.3	32.9	758.6	2433.6	1527.7

Glossary

AHP: Analytical Hierarchy Process

Billion: 10^9

^oC: degrees Celsius

CCS: Carbon Capture and Storage

EOR: Enhanced Oil Recovery

EVPI: Expected Value of Perfect Information

GIS: Geographic Information System

Km: Kilometer

LNG: Liquefied Natural Gas

LPG: Liquefied Petroleum Gas

MEA: Monoethanolamine

Metric ton: 1000 kg or 1 tonne

MJ: Mega Joule

MMV: Measuring, Monitoring and Verification

MPa: Mega Pascals

$MtCO_2$: Mega Tonnes of Carbon Dioxide

Mtpa: Mega Tonnes Per Annum

Pa: Pascals (N/m^2)

PSA: Pressure Swing Absorption

ROW: Right of Way

SMR: Steam Methane Reformer

Tonne: 1000 kilograms

TOPSIS: Technique for Order of Preference by Similarity to Ideal Solution

Tpd: Tonnes per Day

Trillion: 10^{12}

USD: United States Dollar

VSS: Value of the Stochastic Solution

References

Asia-Pacific Economic Cooperation (APEC). 2012. Building capacity for CO_2 capture and storage in the APEC region: A training manual for policy makers and practitioners.

Ambrose, W.A., Breton, C., Holtz, M.H., Núñez-López, V., Hovorka, S. D., Duncan, I. J., 2009, CO_2 source-sink matching in the lower 48 United States with examples from the Texas Gulf Coast and Permian Basin, Environmental Geology, Volume 57, Issue 7, pp 1537–1551.

Bachu, S. 2003. Screening and Ranking Sedimentary Basins for Sequestration of CO_2 in Geological Media in Response to Climate Change. Environmental Geology, Vol. 44, pp 277-289.

Bahadori, A., Vuthaluru, H. B. 2010 Predictive tool for an accurate estimation of carbon dioxide transport properties, International Journal of Greenhouse Gas Control, Vol. 4, pp. 532–536.

Berstad, D., Nekså, P., Anantharaman, R. 2012. Low-temperature CO Removal from Natural Gas, Energy Procedia, Vol. 26, pp. 41-48.

Birge, J. R. and Louveaux. F. 2011. Introduction to Stochastic Programming. New York, NY: Springer.

Bistline, J.E., Weyant, J.P., 2013. Electric sector investments under technological and policy-related uncertainties: a stochastic programming approach, Climatic Change, Vol. 121, Issue 2, pp. 143-160.

Blomen, E., Hendriks, C., Neele, F. 2009. Capture technologies: Improvements and promising developments, Energy Procedia, Vol. 1, Issue 1, pp. 1505-1512.

Buit, L., Ahmad, M., Mallon, W., Hage, F. 2011. CO_2 EuroPipe study of the occurrence of free water in dense phase CO_2 transport, Energy Procedia, Vol. 4, pp. 3056-3062.

Carbon Sequestration Leadership Forum (CSLF). 2017. Enabling Large-scale CCS using Offshore CO_2 Utilization and Storage Infrastructure Developments, CSLF Offshore CO_2-EOR Task Force

Carr, D.L., Wallace, K.J., Yang, C., Nicholson, A.J. 2016. CO_2 Sequestration Capacity Sectors in Miocene Strata of the Offshore Texas State Waters, GCAGS Journal, Vol. 5, pp. 130–140.

Chadwick, A., Arts, R., Eiken, O., 2005. 4D seismic quantification of a growing CO_2 plume at Sleipner, North Sea, Petroleum Geology: North West Europe and Global Perspectives—Proceedings of the 6th Petroleum Geology Conference. pp. 1385-1399.

Chen, W.T., Li, Y.P., Huang, G.H., Chen, X., Li, Y.F. 2010. A two-stage inexact-stochastic programming model for planning carbon dioxide emission trading under uncertainty, Applied Energy, Vol. 87, Issue 3, pp. 1033-1047.

Dijkstra, E. W. 1959. A note on two problems in connexion with graphs. Numerische Mathematik 1, pp. 269–271

Dixon, T., Garrett, J., Kleverlaan, E. 2014. Update on the London Protocol – Developments in Transboundary CCS and on Geoengineering, Energy Procedia, Vol. 63, pp.6623-6628.

European Commission. 2009. Implementation of Directive 2009/31/EC on the Geological Storage of Carbon Dioxide, Guidance Document 3, Criteria for Transfer of Responsibility to the Competent Authority.

Essandoh-Yeddu, J. and Gülen, G. 2009. Economic modeling of carbon dioxide integrated pipeline network for enhanced oil recovery and geologic sequestration in the Texas Gulf Coast region, Energy Procedia, Vol. 1, Issue 1, pp. 1603-1610.

Fimbres Weihs, G.A., Wiley, D.E., Ho, M. 2011. Steady-state optimisation of CCS pipeline networks for cases with multiple emission sources and injection sites: South-east Queensland case study, Energy Procedia, Vol. 4, pp. 2748-2755.

Fimbres Weihs, G.A., Kumar, K., Wiley, D.E. 2014. Understanding the Economic Feasibility of Ship Transport of CO_2 within the CCS Chain, Energy Procedia, Vol. 63, pp. 2630-2637.

Genic, S., Arandjelović, I., Kolendić, P., Jarić, M., Budimir, N., Genić, V. 2011. A Review of Explicit Approximations of Colebrook's Equation, FME Transactions, Vol. 39, pp. 67-71.

Glazewski, K., 2016. Wellbore Integrity, IEAGHG CCS Summer School, Accessed March 2018: http://www.ieaghg.org/docs/General_Docs/Summer_School_2016/Presentations%20for%20web/09_Glazewski_Wellbore%20Integrity.pdf

Global Carbon Capture and Storage Institute (GCCSI). 2009. An Ideal Portfolio of CCS Projects and Rationale for Supporting Projects, L.E.K. Consulting.

Global Carbon Capture and Storage Institute (GCCSI). 2011. Preliminary Feasibility Study on CO_2 Carrier for Ship-based CCS, Chiyoda Report: CCSC-RPT-10-002.

Global Carbon Capture and Storage Institute (GCCSI). 2013. CCS Learning from the LNG Sector, Worley Parsons Report: 401010-01060 – 00-PM-REP-0001.

Global Carbon Capture and Storage Institute (GCCSI). 2014. The Global Status of CCS: 2014, Melbourne, Australia.

Gulf Coast Carbon Center (GCCC). 2013. CO_2 Brine Database. Accessed March 2018: http://www.beg.utexas.edu/gccc/CO_2-data/data-main

Han, J-H. Ryu, J-H., Lee, I-B. 2012. Developing a Two-Stage Stochastic Programming Model for CO_2 Disposal Planning under Uncertainty. Industrial & Engineering Chemistry Research, Vol. 51, Issue 8, pp. 3368-3380.

Han, J-H. and Lee, I-B. 2011a. Development of a scalable infrastructure model for planning electricity generation and CO_2 mitigation strategies under mandated reduction of GHG emission, Applied Energy, Vol. 88, Issue 12, pp. 5056-5068.

Han, J-H. and Lee, I-B. 2011b. Two-Stage Stochastic Programming Model for Planning CO_2 Utilization and Disposal Infrastructure Considering the Uncertainty in the CO_2 Emission, Industrial & Engineering Chemistry Research, Vol. 50, Issue 23, pp. 13435-13443.

Han, J-H. and Lee, I-B. 2013. A Comprehensive Infrastructure Assessment Model for Carbon Capture and Storage Responding to Climate Change under Uncertainty. Industrial & Engineering Chemistry Research, Vol. 52, Issue 10, pp. 3805-3815.

Heddle, G., Herzog H., Klett, M. 2003. The Economics of CO_2 Storage, M.I.T., Report: LFEE 2003-003 RP.

Ho, M.T., Allinson, G.W., Wiley, D.E. 2011. Comparison of MEA capture cost for low CO_2 emissions sources in Australia, International Journal of Greenhouse Gas Control, Vol. 5, Issue 1, pp. 49-60.

Homer, C.G., Dewitz, J.A., Yang, L., Jin, S., Danielson, P., Xian, G., Coulston, J., Herold, N.D., Wickham, J.D., and Megown, K. 2015. Completion of the 2011 National Land Cover Database for the conterminous United States-Representing a decade of land cover change information. Photogrammetric Engineering and Remote Sensing, Vol. 81, pp. 345-354.

International Energy Agency (IEA). 2010. Power Generation from Coal, Measuring and Reporting Efficiency Performance and CO_2 Emissions, OECD/IEA, Paris.

International Energy Agency (IEA). 2011a. Technology Roadmap Carbon Capture and Storage in Industrial Applications, OECD/IEA, Paris.

International Energy Agency (IEA). 2011b. Carbon Capture and Storage Legal and Regulatory Review, OECD/IEA, Paris.

International Energy Agency (IEA). 2012. Energy Technology Perspectives 2012: Pathways to a Clean Energy System, OECD/IEA, Paris.

International Energy Agency (IEA). 2013. Technology Roadmap Carbon capture and storage – 2013 Edition, OECD/IEA, Paris.

International Energy Agency (IEA). 2018. Global Energy & CO_2 Status Report 2017, OECD/IEA, Paris.

International Energy Agency Greenhouse Gas R&D Programme (IEAGHG). 2004. Ship transport of CO_2. IEAGHG, Report No.: PH4/30.

International Energy Agency Greenhouse Gas R&D Programme (IEAGHG). 2006. CO_2 Capture as a Factor in Power Station Investment Decision, Report No.: 2006-8.

International Energy Agency Greenhouse Gas R&D Programme (IEAGHG). 2008. CO_2 Capture in the Cement Industry, IEAGHG, Report No.: 2008/3.

International Energy Agency Greenhouse Gas R&D Programme (IEAGHG). 2009. CCS Site Characterisation Criteria, Report No.: 2009/10.

International Energy Agency Greenhouse Gas R&D Programme (IEAGHG). 2010. Development of a global CO_2 pipeline infrastructure, Report: 2010/13.

International Energy Agency Greenhouse Gas R&D Programme (IEAGHG). 2012. Operating Flexibility of Power Plants with CCS, Report No.: 2012/6.

International Energy Agency Greenhouse Gas R&D Programme (IEAGHG). 2015. Carbon capture and storage cluster projects: review and future opportunities, Report No.: 2015/3.

International Energy Agency Greenhouse Gas R&D Programme (IEAGHG). 2017. Techno-Economic Evaluation of SMR Based Standalone (Merchant) Plant with CCS, 2017/02.

IPCC. 2005. IPCC Special Report on Carbon Dioxide Capture and Storage. Prepared by Working Group III of the Intergovernmental Panel on Climate Change, Cambridge University Press, Cambridge, United Kingdom and New York, NY, USA, 442 pp.

IPCC. 2014. Climate Change 2014: Synthesis Report. Contribution of Working Groups I, II and III to the Fifth Assessment Report of the Intergovernmental Panel on Climate Change. IPCC, Geneva, Switzerland, 151 pp.

Kestenbaum, H., Lange de Oliveira, A., Schmidt, W., Schüth, F., Ehrfeld, W., Gebauer, K., Holger, L., Richter, T., Lebiedz, D., Untiedt, I., Züchner, H. 2002. Silver-Catalyzed Oxidation of Ethylene to Ethylene Oxide in a Microreaction System. Industrial & Engineering Chemistry Research, Vol.41, pp. 710-719.

Kinder Morgan. 2013. Kinder Morgan Transmission Pipeline FERC Gas Tariff Quality Provisions, Kinder Morgan.

King, C.W., Gülen, G., Cohen, S.M., Nuñez-Lopez, V. 2013. The system-wide economics of a carbon dioxide capture, utilization, and storage network: Texas Gulf Coast w/ pure CO_2–EOR flood, Environmental Research Letters, Vol. 8, Number 3.

Kriegler, E., Weyant, J.P., Blanford, G.J. Krey, V., Clarke, L., Edmonds, J., Fawcett, A., Luderer, G., Riahi, K., Richels, R., Rose, S.K., Tavoni, M., van Vuuren, D.P. 2014. The role of technology for achieving climate policy objectives: overview of the EMF 27 study on global technology and climate policy strategies, Climatic Change, Vol. 123, pp. 353-367.

Kuby, M.J., Middleton, R.S., Bielicki, J.M. 2011. Analysis of cost savings from networking pipelines in CCS infrastructure systems, Energy Procedia, Vol 4, pp. 2808-2815.

Kuuskraa, V.A., Godec, M.L., Dipietro, P. 2013. CO_2 Utilization from "Next Generation" CO_2 Enhanced Oil Recovery Technology, Energy Procedia, Vol. 37, pp. 6854-6866.

Lee, S-Y., Lee, J-U., Lee, I-B., Han, J-H. 2017. Design under uncertainty of carbon capture and storage infrastructure considering cost, environmental impact, and preference on risk, Applied Energy, Vol. 189, pp. 725-738.

Leeson, D., Mac Dowell, N., Shah, N., Petit, C., Fennell, P.S. 2017. A Techno-economic analysis and systematic review of carbon capture and storage (CCS) applied to the iron and steel, cement, oil refining and pulp and paper industries, as well as other high purity sources, International Journal of Greenhouse Gas Control, Vol. 61, pp. 71-84.

Leibowicz, B. 2018. The cost of policy uncertainty in electric sector capacity planning: Implications for instrument choice. The Electricity Journal, Vol. 31, pp. 33-41.

Leung, D.Y.C., Caramanna, G., Maroto-Valer, M. 2014. An overview of current status of carbon dioxide capture and storage technologies, Renewable and Sustainable Energy Reviews, Vol. 39, pp. 426-443.

Lindsay, I., Lowe, C., Reddy, S., Bhakta, M., Balkenende, S. 2009. Designing a climate friendly hydrogen plant, Energy Procedia, Vol. 1, Issue 1, 2009, pp. 4095-4102.

Malczewski, J. 2006. GIS-based multicriteria decision analysis: a survey of the literature, International Journal of Geographical Information Science, Vol. 20, Issue 7, pp. 703-726.

Mallon, W., Buit, L., van Wingerden, J., Lemmens, H., Eldrup, N. H. 2013. Costs of CO_2 Transportation Infrastructures, Energy Procedia, Vol. 37, pp. 2969-2980.

McCollum, D.L. and Ogden, J.M. 2006. Techno-Economic Models for Carbon Dioxide Compression, Transport, and Storage, University of California-Davis, UCD-ITS-RR-06-14.

McCoy, S.T., Rubin, E.S. 2008. An engineering-economic model of pipeline transport of CO_2 with application to carbon capture and storage, International Journal of Greenhouse Gas Control, Vol. 2, Issue 2, pp. 219-229.

Meckel, T.A., Trevino, R., Hovorka, S.D. 2017. Offshore CO_2 Storage Resource Assessment of the Northern Gulf of Mexico, Energy Procedia, Vol. 114, pp. 4728-4734.

Melzer, S. L. 2011. Emergence Of Residual Zones, Price And Supply Factors Usher In New Day In CO_2 EOR, The American Oil and Gas Reporter, Accessed March 2018: https://www.aogr.com/magazine/cover-story/emergence-of-residual-zones-price-and-supply-factors-usher-in-new-day-in-co

Michael, K., Golab, A., Shulakova, V., Ennis-King, J., Allinson, G., Sharma, S., Aiken, T. 2010. Geological storage of CO_2 in saline aquifers—A review of the experience

from existing storage operations, International Journal of Greenhouse Gas Control, Volume 4, Issue 4, pp. 659-667.

Middleton, R.S. and Bielicki, J.M. 2009. A scalable infrastructure model for carbon capture and storage: SimCCS, Energy Policy, Vol. 37, Issue 3, pp. 1052-1060.

Middleton, R.S., Kuby, M.J., Bielicki, J.M. 2012a. Generating candidate networks for optimization: The CO_2 capture and storage optimization problem, Computers, Environment and Urban Systems, Vol. 36, Issue 1, pp. 18-29.

Middleton, R.S., Kuby, M.J., Wei, R., Keating, G.N., Pawar, R.J. 2012b. A dynamic model for optimally phasing in CO_2 capture and storage infrastructure, Environmental Modelling & Software, Vol. 37, pp. 193-205.

Morbee, J., Serpa, J., Tzimas, E. 2011. Optimal planning of CO_2 transmission infrastructure: The JRC InfraCCS tool, Energy Procedia, Vol. 4, pp. 2772-2777.

National Energy Technology Laboratory (NETL). 2014. Carbon Dioxide Transport and Storage Costs in NETL Studies. DOE/NETL-2013/1614.

National Energy Technology Laboratory (NETL). 2015a. A Review of the CO_2 Pipeline Infrastructure in the US. DOE/NETL-2014/1681.

National Energy Technology Laboratory (NETL). 2015b. Carbon Storage Atlas, Fifth Edition. DOE/NETL-2015/1709.

National Energy Technology Laboratory (NETL). 2017. Siting and Regulating Carbon Capture, Utilization and Storage Infrastructure, Workshop Report.

Nemeth, K.J. 2006. Southeast Regional Carbon Sequestration Partnership (SECARB), DOE Award: DE-FC26-03NT41980.

Norwegian Ministry of Petroleum and Energy. 2016. Feasibility Study for Full-Scale CCS in Norway, Accessed March 2018: https://www.gassnova.no/en/Documents/Feasibilitystudy_fullscale_CCS_Norway_2016.pdf

National Park Service (NPS). 2017. Administrative Boundaries of National Park System Units - National Geospatial Data Asset (NGDA). NPS National Parks Dataset. NPS - Land Resources Division.

Ogden, J. M. 2004. Conceptual Design of Optimized Fossil Energy Systems with Capture and Sequestration of Carbon Dioxide. United States Department of Energy National Energy Technology Laboratory Report.

Ozaki, M., Ohsumi, T., Kajiyama,R. 2013. Ship-based Offshore CCS Featuring CO_2 Shuttle Ships Equipped with Injection Facilities, Energy Procedia, Vol. 37, pp. 3184-3190.

Parker, N. 2004. Using Natural Gas Transmission Pipeline Costs to Estimate Hydrogen Pipeline Costs, University of California-Davis, UCD-ITS-RR-04-35.

Perpiñá, C., Alfonso, D., Pérez-Navarro, A., Peñalvo, E., Vargas, C., Cárdenas, R., 2009, Methodology based on Geographic Information Systems for biomass logistics and transport optimisation, Renewable Energy, Volume 34, Issue 3, pp. 555-565.

Rackley, S. A. 2010. Carbon capture and storage. Burlington, MA: Butterworth-Heinemann.

Rockett, G., Machado, C., Medina Ketzer, J., Centeno, C., 2011, The CARBMAP project: Matching CO_2 sources and geological sinks in Brazil using geographic information system, Energy Procedia, Volume 4, pp. 2764-2771.

Roussanaly, S., Bureau-Cauchois, G., Husebye, J. 2013 Costs benchmark of CO_2 transport technologies for a group of various size industries, International Journal of Greenhouse Gas Control, Vol. 12, pp. 341-350.

Rubin, E.S., Davison, J.E., Herzog, H.J. 2015. The cost of CO_2 capture and storage, International Journal of Greenhouse Gas Control, Volume 40, pp. 378-400

Sánchez-Lozano, J., Teruel-Solano, J., Soto-Elvira, P., García-Cascales, M. S., 2013, Geographical Information Systems (GIS) and Multi-Criteria Decision Making (MCDM) methods for the evaluation of solar farms locations: Case study in south-eastern Spain, Renewable and Sustainable Energy Reviews, Volume 24, pp. 544-556.

Seni, S. J., Hentz, T. F., Kaiser, W. R., Wermund Jr., E. G. 1997. Atlas of northern Gulf of Mexico gas and oil reservoirs: Volume 1. Miocene and older reservoirs: University of Texas at Austin, Bureau of Economic Geology, Gas Research Institute, Department of Energy, and Minerals Management Service, 199 p.

Serpa, J., Morbee, J., Tzimas. E. 2011. Technical and Economic Characteristics of a CO_2 Transmission Pipeline Infrastructure. Luxembourg: Publications Office of the European Union. Accessed March 2018 http://publications.jrc.ec.europa.eu/repository/bitstream/111111111/16038/1/reqno_jrc62502_aspublished.pdf

Smith, C. E. 2009. Special Report: Pipeline profits, capacity expansion plans grow despite increased costs, Oil and Gas Journal, Accessed March 2018: https://www.ogj.com/articles/print/volume-107/issue-34/Transportation/special-report-pipeline-profits-capacity-expansion-plans-grow-despite-increased-costs.html

Smith, C. E. 2014. Crude oil pipeline growth, revenues surge; construction costs mount, Oil and Gas Journal, Accessed March 2018: https://www.ogj.com/articles/print/volume-112/issue-9/special-report-pipeline-economics/crude-oil-pipeline-growth-revenues-surge-construction-costs-mount.html

Smith, C. E. 2017. Oil pipeline profits soar, natgas net softens, Oil and Gas Journal, Accessed March 2018: https://www.ogj.com/articles/print/volume-115/issue-

10/special-report-pipeline-economics/oil-pipeline-profits-soar-natgas-net-softens.html

Sultana, A. and Kumar, A., 2012, Optimal siting and size of bioenergy facilities using geographic information system, Applied Energy, Volume 94, pp. 192-201.

Texas Commission on Environmental Quality (TCEQ). 2012. Condensate Tank Oil and Gas Activities, Texas Commission on Environmental Quality Air Quality Division, Eastern Research Group Inc.

Texas Parks and Wildlife Division (TPWD). 2016. State Park Boundaries, Downloadable Data Collection: Texas Parks and Wildlife Division.

Treviño, R. H., and Meckel, T. A. 2017. Geological CO_2 Sequestration Atlas of Miocene Strata, Offshore Texas State Waters: The University of Texas at Austin, Bureau of Economic Geology, Report of Investigations No. 283, 74 p.

U.S. Army Corps of Engineers. 2018. U.S. Waterway Data: Waterway Network Link Commodity Data, Navigation Data Center.

U.S. Census Bureau. 2015. TIGER Geodatabases – Roads National Geodatabase.

U.S. Department of Transportation (USDOT). 2017. National Transportation Atlas Database – Railroad Lines.

U.S. Energy Information Administration (EIA). 2018. Electric Power Monthly with Data for January 2018. U.S. Department of Energy, Washington D.C.

U.S. Environmental Protection Agency (USEPA) and the U.S. Geological Survey (USGS), 2012, National Hydrography Dataset Plus – NHDPlus, Version 2.

U.S. Geological Survey (USGS). 2017. 1/3rd arc-second Digital Elevation Models (DEMs) - USGS National Map 3DEP, Downloadable Data Collection: U.S. Geological Survey.

Uyan, M., 2013, GIS-based solar farms site selection using analytic hierarchy process (AHP) in Karapinar region, Konya/Turkey, Renewable and Sustainable Energy Reviews, Volume 28, pp. 11-17.

Vandeginste, V., Piessens, K. 2008. Pipeline design for a least-cost router application for CO_2 transport in the CO_2 sequestration cycle, International Journal of Greenhouse Gas Control, Vol. 2, Issue 4, pp 571-581.

Wenying, C., Lingyan, H., Xing, X., Jiyong, C., Liang S. 2011. GIS based CCS source-sink matching models and decision support system, Energy Procedia, Vol. 4, pp. 5999-6006.

Zero Emissions Platform (ZEP). 2011a. The Costs of CO_2 Capture: Post-Demonstration CCS in the EU, European Technology Platform for Zero Emission Fossil Fuel Power Plants, Brussels.

Zero Emissions Platform (ZEP). 2011b. The Costs of CO_2 Transport: Post-Demonstration CCS in the EU, European Technology Platform for Zero Emission Fossil Fuel Power Plants, Brussels.

Zero Emissions Platform (ZEP). 2011c. The Costs of CO_2 Storage: Post-Demonstration CCS in the EU, European Technology Platform for Zero Emission Fossil Fuel Power Plants, Brussels.

Zhou, D., Zhang, Y., Haszeldine, S. 2014, Engineering Requirements for Offshore CO_2 Transportation and Storage: A Summary Based on International Experiences, UK-China (Guangdong) CCUS Centre.

Zigrang, D.J., Sylvester, N.D. 1982. Explicit approximations to the solution of Colebrook's friction factor equation, AIChE Journal, Vol. 28, No. 3, pp. 514-515.